ORNL/TM-2021/2293

Connected Loads – Grid Connected Appliances: Commercial Refrigeration System Fault Detection and Diagnostics

Oct. 2021

OAK RIDGE National Laboratory

ORNL IS MANAGED BY UT-BATTELLE LLC FOR THE US DEPARTMENT OF ENERGY

DOCUMENT AVAILABILITY

Reports produced after January 1, 1996, are generally available free via US Department of Energy (DOE) SciTech Connect.

Website www.osti.gov

Reports produced before January 1, 1996, may be purchased by members of the public from the following source:

National Technical Information Service
5285 Port Royal Road
Springfield, VA 22161
Telephone 703-605-6000 (1-800-553-6847)
TDD 703-487-4639
Fax 703-605-6900
E-mail info@ntis.gov
Website http://classic.ntis.gov/

Reports are available to DOE employees, DOE contractors, Energy Technology Data Exchange representatives, and International Nuclear Information System representatives from the following source:

Office of Scientific and Technical Information
PO Box 62
Oak Ridge, TN 37831
Telephone 865-576-8401
Fax 865-576-5728
E-mail reports@osti.gov
Website https://www.osti.gov/

This report was prepared as an account of work sponsored by an agency of the United States Government. Neither the United States Government nor any agency thereof, nor any of their employees, makes any warranty, express or implied, or assumes any legal liability or responsibility for the accuracy, completeness, or usefulness of any information, apparatus, product, or process disclosed, or represents that its use would not infringe privately owned rights. Reference herein to any specific commercial product, process, or service by trade name, trademark, manufacturer, or otherwise, does not necessarily constitute or imply its endorsement, recommendation, or favoring by the United States Government or any agency thereof. The views and opinions of authors expressed herein do not necessarily state or reflect those of the United States Government or any agency thereof.

ORNL/TM-2021/2293

BTO Project 03.02.07.71
FY21 Final Report

CONNECTED LOADS- GRID CONNECTED APPLIANCES: COMMERCIAL REFRIGERATION SYSTEM FAULT DETECTION AND DIAGNOSTICS

Yanfei Li
Jian Sun
Teja Kuruganti
Piljae Im
Brian Fricke
Jeff Munk
Yeonjin Bae
Mahabir Bhandari

Oct. 2021

Prepared by
OAK RIDGE NATIONAL LABORATORY
Oak Ridge, TN 37831-6283
managed by
UT-BATTELLE, LLC
for the
US DEPARTMENT OF ENERGY
under contract DE-AC05-00OR22725

CONTENTS

LIST OF FIGURES

LIST OF TABLES

EXECUTIVE SUMMARY

As one of the most energy-intensive end-uses in the commercial buildings sector, supermarkets consume around 50 kWh/ft^2 (or 537.6 kWh/m^2) of electricity annually, or more than 2 million kWh of electricity per year for a typical store. The biggest consumer of energy in a supermarket is its refrigeration system, which accounts for 40–60% of its total electricity usage and is equivalent to about 2–3% of the total energy consumed by commercial buildings in United States, or around 0.5 quadrillion Btu (or 0.53 quadrillion KJ). Also, the supermarket refrigeration system is one of the biggest consumers of refrigerants. Current supermarket refrigeration systems rely on high global warming potential hydrofluorocarbon refrigerants. Reducing refrigerant usage or using environment friendly alternatives can result in significant climate benefits. Transcritical CO2 refrigeration systems have attracted more attention in recent years because of their zero-carbon emission advantages compared with traditional refrigerants. These systems are widely used in commercial buildings such as supermarkets. The refrigeration system can also be adapted to handle flexible building loads and be integrated into grid response transactive control to balance the supply and demand of the electric grid. Even minor improvements in the efficiency and operational reliability of supermarket refrigeration systems can create significant value in terms of saving energy, improving food quality, protecting the environment, reducing carbon footprint, and enhancing electric grid resilience.

Fault detection and diagnostics (FDD) techniques can be used to support refrigeration system operators in achieving these benefits. However, compare to heating, ventilation and air-conditioning and refrigeration system which has attracted extensive FDD studies for decades, FDD of supermarket refrigeration systems, especially for low GWP refrigerant supermarket refrigeration system, has not gained enough attention from researchers. One of the key challenges is lack of available testing datasets to benchmark the system performance and record the faulted performance to system FDD research. This study conducted both experimental and simulation studies of commercial refrigeration system FDD. The experimental study selects several common faults of supermarket refrigeration systems, including displace case door open, ice accumulation, expansive valve failure, and fan failure, to conduct experimental study to identify their fault characteristics, benchmark their faulted performance, then create a FDD characteristics matrix to support the development of supermarket refrigeration system FDD methods and field automated FDD implementation. Based on experimental results, fault models (gray-box format) regarding the power consumption and supply air temperature were proposed for low- and high-temperature display cases, respectively. The models cover: ice accumulation on evaporator coil, evaporator fan partial failure, expansion valve failure, display door open, and condenser blockage. These fault models were calibrated with test data, and the modeling accuracies were in good agreement with measurement datasets based on the root mean square error. Then these fault models were implemented through PythonEMS of the EnergyPlus platform. In addition, FDD algorithms were developed using these developed fault models and applied for both field measurement and simulated data.

1. INTRODUCTION

As the most energy-intensive end-uses in the commercial buildings sector, supermarkets consume around 50 kWh/ft^2 (or 537.6 kWh/m^2) of electricity annually [1], which is more than 2 million kWh of electricity per year for a typical supermarket store. As the biggest consumer of energy in a supermarket, the refrigeration system accounts 40–60% of total supermarket electricity usage, which is about 2–3% of the total energy consumed by commercial buildings in United States, or around 0.5 quadrillion Btu (or 0.53 quadrillion KJ) [2]. Also, the supermarket refrigeration system is one of the biggest consumers of refrigerants. Current supermarket refrigeration systems rely on high global warming potential hydrofluorocarbon refrigerants. Reducing refrigerant usage or using environment friendly refrigerant alternatives can result in significant climate benefits. In addition, the supermarket refrigeration system can be adapted to handle flexible building loads and be integrated into grid response transactive control to balance the supply and demand of the electric grid [3]. Thus, even a small improvement in the operational reliability and efficiency of supermarket refrigeration systems can create significant values in terms of saving energy, carbon footprint reduction, improving food quality, protecting the environment, and enhancing the electric grid resilience.

In recent years, more transcritical CO2 refrigeration systems have been adopted by supermarkets. These systems are characterized by multiple benefits compared with traditional direct expansion refrigeration systems: (1) higher volumetric refrigerating capacity than other refrigerants such as chlorofluorocarbon, hydrochlorofluorocarbon, hydrofluorocarbon, and hydrocarbon refrigerants [4]; (2) no ozone depletion potential; (3) zero global warming potential; and (4) nontoxic, nonflammable, and inexpensive components and emissions. One study [4] concluded that the lower ratio of media pressure and high-temperature compressor efficiency could lead to an increased coefficient of performance for a booster CO2 transcritical system. Another study [6] found that the CO2 refrigeration system could achieve 30% efficiency in different climate zones if ejectors and heat recovery components are added into the system. In da Silva et al. (2012), the authors compared the cascade CO2 refrigeration systems [7] with the traditional cascade refrigeration systems(R404a and R22), and they concluded that CO2 refrigeration systems have multiple merits, such as compactness, less electricity consumption, and lower environment impacts.

Fault detection and diagnostics (FDD) techniques have been used to support supermarket refrigeration system operators in achieving these benefits. BehFar et al. [8, 9] presented two automated fault detection and diagnosis approaches, a data-driven method and a rule-based method, to realize the benefits of Automated FDD, such as prevention of energy waste, system damage, and food loss in supermarket setting. Their study found that the rule-based method is suitable for scenarios in which controlled variables are selected as the performance index, whereas the data-driven method performs better in the detection of energy consumption variation. Yang et al. [10, 11] proposed an extended Kalman Filter based fault detection isolation method to detect all concerned faults correctly for the purpose of improving the efficiency and reliability of supermarket refrigeration systems. Like other vapor compression systems, typical faults that occur in supermarket refrigeration systems include refrigerant leakage, lubrication issues, evaporator icing or fouling, condenser fouling, control system problems, compressor inefficiency, condenser fan or motor issues, evaporator fan or motor issues, control valve malfunctioning, cabinet glass door frosting, liquid line restrictions, etc. Kim [12] conducted an experimental study of four common faults found in a variable-speed vapor compression system: compressor fault, condenser fault, evaporator fault, and refrigerant leakage. According to Kim's test results, the system parameters are insensitive to the compressor fault for a variable-speed compressor system as the compressor speed can be controlled to compensate for the faults. Tassou and Grace [13] developed a FDD strategy using an artificial intelligence and real-time performance monitoring approach for refrigerant leakage detection and diagnosis to overcome difficulties associated with the inability to

detect gradual leakage and to carefully determine a sensor's optimum location. Given the limited amount of quality data available, Zhao et al. [14] used a field test environment, instead of a laboratory environment, to evaluate some common chiller faults: reduced water flow rate fault, improper refrigerant charge fault, condenser fouling faults, and non-condensable gas in the refrigerant fault. Kocyigit et al. [15] investigated several faults: compressor failure, restricted filter-dry, restricted electronic expansion valve (EXV), compressor valve leakage, undercharging, overcharging, a dirty condenser, and evaporator fan failure. They categorized the faults into two types: hard failures and soft failures. BehFar et al. [16] investigated supermarket equipment characteristics and common operating faults based on data collected through expert surveys, facility management system messages, service calls, and service records. According to their study, the most commonly occurring faults are refrigerant leakage/undercharge/overcharge, oil problems, evaporator iced-up/fouling, control system problems, condenser fouling, compressor inefficiency, condenser fan or fan motor problems, evaporator fan or fan motor problems, the interaction of HVAC and refrigeration systems, control valves problems, cabinet glass door frosting, and liquid line restriction. Among these faults, control system problems, refrigerant leakage/undercharge/overcharge, and compressor problems are the three most costly faults to repair.

However, compare to other building HVAC&R equipment and systems [17,18,19,20], such as air handling units (AHUs), roof top unit (RTUs), package air-conditioning, chillers, heat pumps, HVAC controls, furnaces, lighting, supermarket refrigeration systems have not attracted sufficient attention from the researchers to conduct FDD studies. This is especially true for low-GWP refrigerant supermarket refrigeration system which has some unique characteristics in terms of FDD, such as high discharge pressure, a multistage compression system, a frequent defrost cycle for low-temperature evaporators, high air infiltration on medium-temperature open display cases, and doored display cases. One of the key challenges is lack of available datasets to benchmark the system performance and record the faulted performance to support the low GWP refrigerant supermarket refrigeration system FDD research. This study is to fulfil this gap through investigating a few common faults of low-GWP refrigerant, CO_2 in this case, supermarket refrigeration systems experimentally, and identifying the faults characteristics, benchmarking the faulted performance, then create FDD characteristics matrix to provides a foundation for the development of supermarket refrigeration system FDD methods and field automated FDD implementation.

In general, three approaches to fault modeling [21], including black-box, gray-box, and white-box, are used for development of refrigeration system FDD methods. The black-box approach normally uses machine learning (data-driven) algorithms [22], but it lacks physical details in the modeling. The white-box approach is time-consuming and labor-intensive, although it has the best fidelity [23,24]. The gray-box approach combines the strengths of both the black-box and white-box methods, preserving major modeling fidelity with less effort [25]. This study uses the gray-box approach for fault modeling development for CO2 transcritical systems. Multiple sets of experiments were conducted for both the fault scenarios and baseline (fault-free) scenarios [26]. This study proposed multiple fault models for supermarket transcritical CO2 refrigeration systems based on experimental datasets. These fault models were calibrated and demonstrated in a simulation environment for fault detection and diagnostics (FDD) purposes

The remaining sections of this report is organized as follows. In Section 2, experimental study elaborates the test hardware, fault experiment, results analysis and FDD characteristics matrix. Section 3 is modeling and simulation study which describes the modeling methods, creates the baseline and fault models, calibrates and validate these models, and implement them with EnergyPlus through pythonEMS. FDD framework and algorithms are discussed in section 4 which also present the results of applying the proposed FDD algorithms for the lab test data. The section 5 summarizes the study and recommend future studies.

2. EXPERIMENTAL STUDY

2.1 TEST HARDWARE

Laboratory setup for supermarket refrigeration system (Figure 1) consists of a CO_2 compressor rack, MT and LT refrigerated display cases, an air-cooled gas cooler, flash tank, expansion valves (high, medium, low pressure), flash gas control valve, and instrumentation. The overall cooling capacity of this commerical refrigeration system is approximately 43 kW with approximatly LT cooling capcity of 9.2 kW at -30°C evaporating temperature and approximatly MT cooling capacity of 33.8 kW at -6.7°C evaporating tempertaure.

Figure 1. Supermarket refrigeration system

The compressor rack contains two LT compressors and three MT compressors using CO_2 refrigerant. Each set of compressors consists of one primary variable-speed compressor (capable of modulating capacity from 10% to 100%) and one or two secondary fixed-speed compressors. The LT compressors operate in a subcritical mode, and the MT compressors can operate in both a subcritical mode and supercritical mode. When the refrigeration load is low, the load is handled by a primary variable-speed compressor that can modulate its capacity according to the load demand, and the secondary fixed-speed compressor is turned off. If the load exceeds the capacity of the primary variable-speed compressor, the secondary fixed-speed compressor is brought online, and the primary variable-speed compressor modulates its capacity to match the load. The target suction pressures (or suction saturation temperatures) are set based on the coldest temperature required by the display cases that those compressors are serving (either MT or LT). Each display case has a temperature setpoint, and the refrigerant flow to the evaporator coil of the case is modulated to maintain this temperature. Therefore, it is possible to control the refrigeration system power consumption by changing these setpoints in addition to more traditional on/off means like shutting off a compressor or compressors or shutting off refrigerant flow to one or more

display cases. Each of these "control levers" will result in different power and thermal responses of the system. Specifications for the compressors are shown in Table 1.

Table 1. Compressor specifications for laboratory-scale refrigeration system.

Compressor type	Temperature level	Capacity control	Model	Refrigerating capacity, kBtu hr^{-1} (kW)*	Power (kW)*
Reciprocating	LT	Fixed	2KSL-1K	19.0 (5.57)	1.34
Reciprocating	LT	Fixed	2MSL-07K	12.0 (3.52)	0.82
Reciprocating	MT	Variable	4MTC-10K	38.0 (11.1)	9.66
Reciprocating	MT	Fixed	4MTC-10K	39.0 (11.4)	9.72
Reciprocating	MT	Fixed	4MTC-7K	38.5 (11.3)	9.4

*Refrigerating capacity and power are given for the following operating conditions using R-744 (CO_2):
LT: -22°F (-30°C) evaporating temperature, 20°F (-6.7°C) condensing temperature
MT: 20°F (-6.7°C) evaporating temperature, 100°F (38°C) condensing temperature

The LT load consists of one 4-door vertical display case 10 ft (3.0 m) long and a false load provided by a plate heat exchanger, two electric heaters, and glycol loop. The rated capacity of the 4-door display case is 5,700 Btu hr^{-1} (1,670 W), and the false load is approximately 20,500 Btu hr^{-1} (6,000 W). The MT load consists of one open vertical display case 8 ft long (2.4 m) and a false load provide by a plate heat exchanger, nine electric heaters, and a glycol loop. The rated capacity of the open display case is 9,600 Btu hr^{-1} (2,810 W), and the false load is approximately 92,000 Btu hr^{-1} (27,000 W). Specifications for the display cases are shown in Table 2.

Table 2. Specifications for refrigerated display cases.

	LT Display Case	MT Display Case
Model Number	6RZLH	O5DM-NRG
Type	4-door, vertical multi-deck	Open, vertical multi-deck
Length	10 ft (3.0 m)	8 ft (2.4 m)
Rated Capacity	5,700 Btu hr^{-1} (1,670 W)	9,600 Btu hr^{-1} (2,810 W)
Fan Amperage	0.93 amps	0.75 amps
Lighting Amperage	0.90 amps	0.40 amps
Anti-Sweat Heater Amperage	7.99 amps	N/A
Defrost Type	Electric	Off-cycle
Defrost Amperage	16.29 amps	N/A

The Luvata (model LGV8812) air-cooled gas cooler is used to reject heat from the refrigeration system by receiving discharge refrigerant vapor from the compressor rack, condensing or cooling the refrigerant, and discharging it into a flash tank. The rated heat rejection capacity of this air-cooled gas cooler is 268,000 Btu hr^{-1} (78.5 kW) for CO_2 at an entering temperature of 242°F (117°C) and an exit gas temperature of 97.5°F (36.4°C).

The commercial refrigeration system was fully instrumented to measure its performance. As shown in Figure 2, the measurements include refrigerant temperature and pressure at the inlet and outlet of major components, such as compressors, display cases, false load heat exchangers, expansion valves, and the gas cooler, as well as refrigerant mass flow rate through the various loads, and power consumption of compressors, gas cooler fans, false load heaters, defrost heaters, and display case fans.

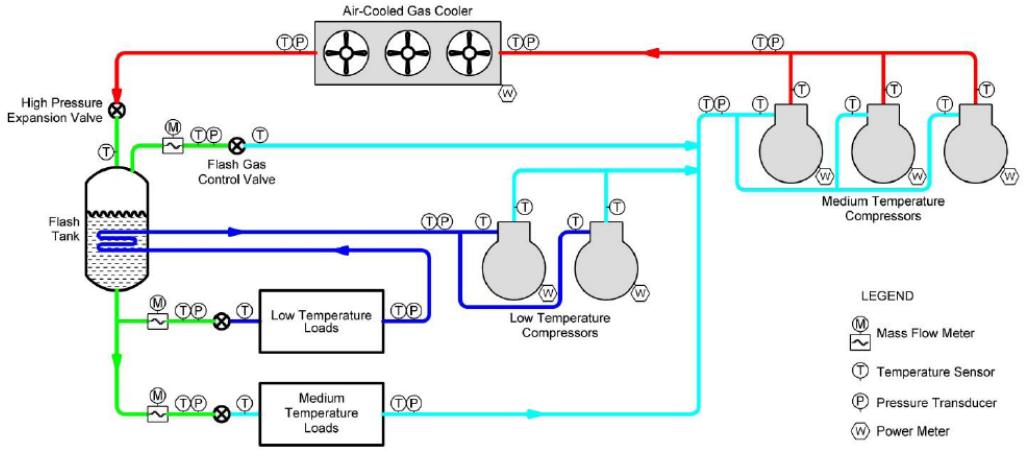

Figure 2. Supermarket refrigeration system diagram [26]

2.2 FAULT EXPERIMENT AND ANALYSIS

Since the supermarket refrigeration systems are generally required to be run almost continuously, detection of the potential faults in early stage is critical to prevent them from escalating into serious issues. The commonly occurring faults of supermarket refrigeration systems can be categorized into three groups: control and operational faults, device faults, and sensor faults. Control and operational faults are resulted from inappropriate control logics, incorrect control settings or operational mistakes, such as display case overstocking, evaporator air path blockage, condenser air path blockage, evaporator coil frost accumulation, defrost heater malfunction, excessive infiltration to the display case, refrigerant leakage/undercharge/overcharge, display-case door left open by mistake. Devices faults are caused by failure or malfunction of individual component, either mechanical or electronic, which include evaporator or condenser fan motor failure, suction side restriction, valve failure, compressor failure, condenser fouling. The manufacture installed sensors in supermarket refrigeration system are generally pressure transducers and temperature thermostats. Several common sensor faults are compressor suction pressure sensor fault, compressor discharge temperature sensor fault, leaving evaporator temperature sensor fault, evaporator supply/return air sensor fault.

In this study, we select four faults of a supermarket refrigeration system to test in an experimental environment and investigate their impacts on the system performance. Four selected faults of supermarket refrigeration systems are display case door open, ice accumulation, expansion valve failure, and fan failure. These four faults are among the most common faults in supermarket refrigeration system and contribute more than 75% of faults which lead the equipment/system failure [16].

Although the tested supermarket refrigeration system has been fully instrumented with pressure transducers, thermocouples, and mass flow meters, and power meters, the impacts of four selected faults on the system are primarily on the compressors, evaporators, and condensers. Open LT display case door left open, ice accumulation, and LT evaporator expansion valve failure primarily influenced LT evaporator operation characteristics. The MT evaporator fan motor failure had significant effects on the MT evaporator performance. All influenced the LT/MT compressor operation through changing the LT/MT compressor suction and discharge refrigerant states. Therefore, these variables list as below,

either measured directly or calculated indirectly, were selected to demonstrate the characteristics of fault events.

Variables representing compressor characteristics:

- LT/MT compressor discharge temperature
- LT/MT compressor discharge pressure
- LT/MT compressor suction temperature
- LT/MT compressor suction pressure
- LT/MT compressor power

Variables representing evaporator characteristics:

- LT/MT evaporator supply air temperature
- LT/MT evaporator return air temperature
- Air temperature difference across LT/MT evaporator
- LT/MT evaporator approach temperature
- LT/MT evaporator exiting superheat temperature

Variables representing condenser characteristics:

- Condenser inlet air temperature
- Condenser outlet air temperature
- Air temperature difference across condenser
- Condenser approach temperature
- Condenser fan power

For each fault test, a fault-free test, with operating conditions similar to those of a fault test, was conducted to service as baseline case for comparison purpose. The fault tests were compared with baseline tests to evaluate the fault performance. The details of experiments and a comparative analysis of four selected faults are given as following.

2.2.1 Fault Test 1: LT display case door open

Leaving display case door open accidentally is not unusual event during shopping in supermarket. In this test, one of the four doors in a LT display case is left open slightly, to mimic an actual situation in which a shopper neglects to close a display case door completely or when a display case door becomes stuck open accidentally. The test is conducted at -25.6 °F (−32°C) of LT compressor suction refrigerant temperature setpoint, −6°F (−21°C) of LT display case discharge air temperature setpoint, 16 °F (-8.9 °C) of MT compressor suction refrigerant temperature setpoint, 30°F (−1.1°C) of MT display case discharge air temperature setpoint and 72°F (22°C) of Indoor air temperature.

The performance of the baseline test is compared with that of the open LT display case door fault test in Fig. 3. According the test results, this LT display case door open fault introduces significant changes on the LT evaporator return air temperature, LT compressor suction temperature, superheat temperature, MT compressor discharge temperature and pressure, and LT compressor power consumption, specifically as below,

- LT evaporator return air temperature immediately rises (Fig. 3b) after the door opens due to warmer infiltration air from outside of displace case. However, the supply air temperature maintains the setpoint with no significant change (Fig. 3a). one of reasons is because the controls increase the refrigerant flow to give additional cooling to counteract the infiltration load introduced by opened door.

- During the defrost cycle, both supply and return air temperatures rise and reach higher temperature

limits than the baseline case (Fig. 3a and 3b). Also, the supply air temperature increases at a much faster rate than the return air temperature, which causes a larger increase in air temperature difference across the LT evaporator under defrost conditions.

- When the display case door opens, both the MT compressor discharge temperature and pressure increase to a moderate level (Fig. 3d and 3e). Clearly, the open door fault calls for more cooling load and results in an increase in power consumption (Fig. 3h), and the compressor needs to work harder to meet the demand, which leads to an increase in discharge temperature and pressure.

- Both the LT compressor suction temperature and superheat temperature drop when the open LT display case door fault occurs (Fig. 3f and 3g).

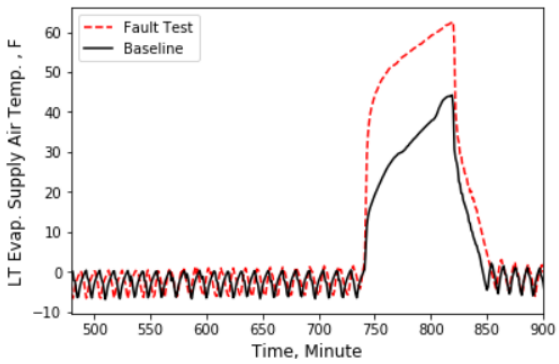

Fig. 3.a: LT evaporator supply air temperature

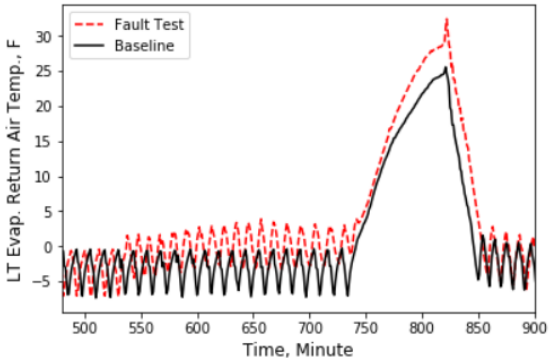

Fig. 3.b: LT evaporator return air temp.

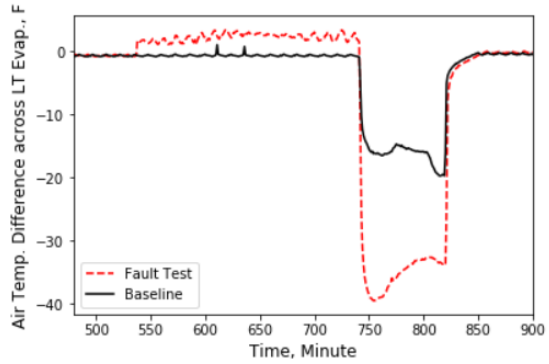

Fig. 3c: Air temperature drop/rise across evaporator

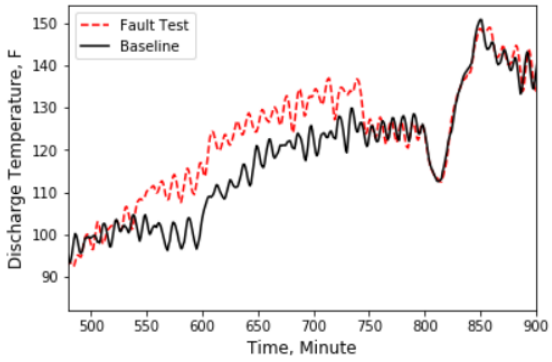

Fig. 3d: MT compressor discharge temperature

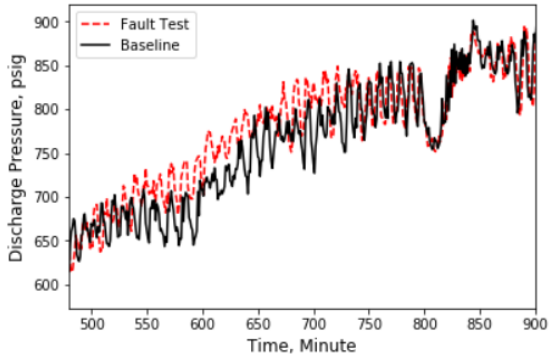

Fig. 3e: MT compressor discharge pressure

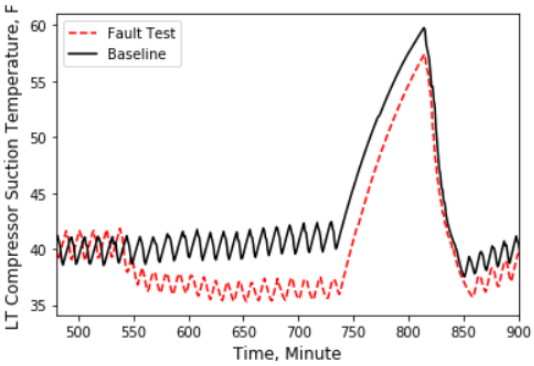

Fig. 3f: LT compressor suction temperature

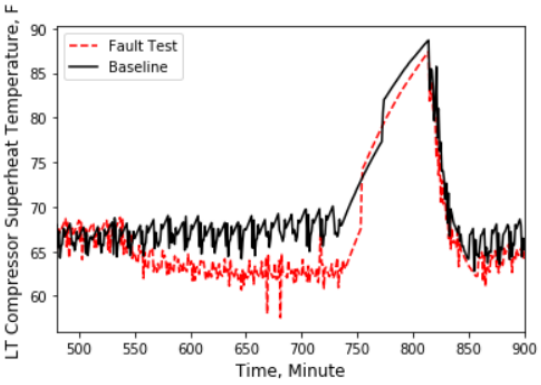

Fig. 3g: LT compressor superheat temperature

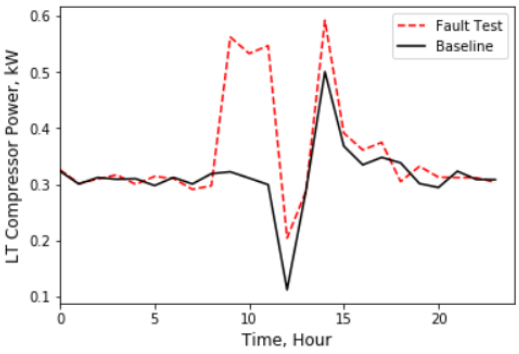

Fig. 3h: LT compressor power consumption

Figure 3. Performance comparison of a baseline test and fault test 1.

2.2.2 Fault Test 2: Ice accumulation on LT display case evaporator coil

Ice accumulation on the evaporator coil surface is one of most common issues faced by many supermarket refrigeration systems. In this ice accumulation fault test, the refrigeration system defrost frequency was manually reduced or set to no defrost. The ice was building up gradually over four days period. The experimental results are compared with the fault-free baseline test as shown in Fig. 4(a–f)

- As ice builds up on the LT evaporator coil surface, the overall heat transfer coefficient of the coil will decrease. To counteract the reduction in heat transfer, the refrigerant flow through the coil increases to handle the load and maintain the return air temperature at its setpoint (Fig. 4b). The accumulated ice blocks the air path and reduces the actual airflow across the coil, which causes the supply air temperature to increase (Fig. 4a) and the air temperature difference across the LT evaporator to become greater (Fig. 4c). Figure 4d shows the gradual increase in air temperature difference across the LT evaporator over four days of operation.

- The LT evaporator approach temperature slightly drops as ice builds up on the evaporator coil, as shown in Fig. 4j (before defrost cycle). The defrost process will drive the approach temperature close to a normal approach temperature as in the baseline test case, as shown in Fig. 4e after the defrost cycle.

Other performance variables, such as LT compressor discharge temperature and pressure, LT compressor suction temperature, the air temperature difference across the condenser, and LT/MT compressor power consumption, have been noticed with little impact by the ice accumulation fault during the test period.

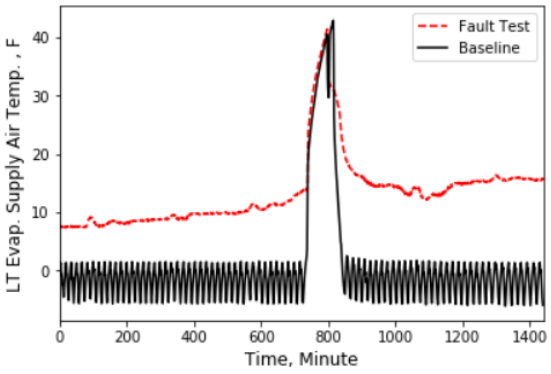

Fig. 4a: LT evaporator supply air temperature

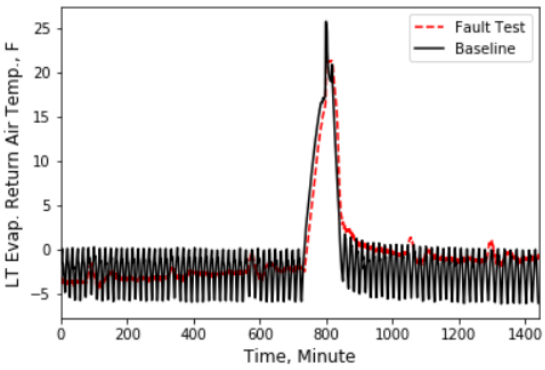

Fig. 4b: LT evaporator return air temperature

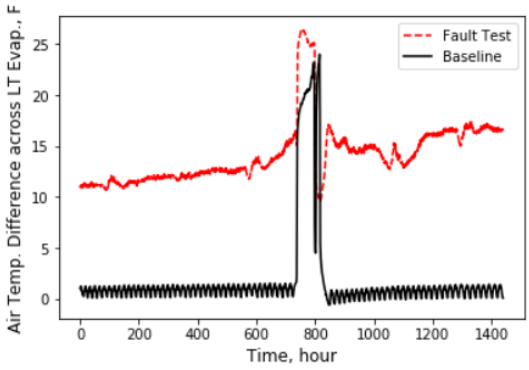

Fig. 4c: Air temp. drop/rise across evaporator

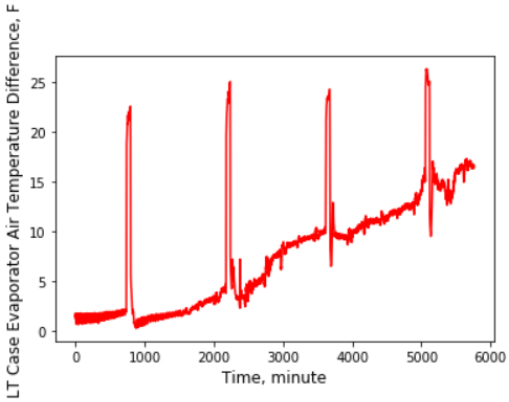

Fig. 4d: Air temp. difference across LT evap. over 4 days

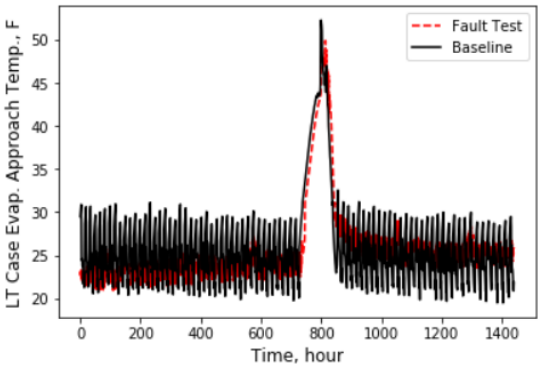

Fig. 4e: LT evaporator approach temperature

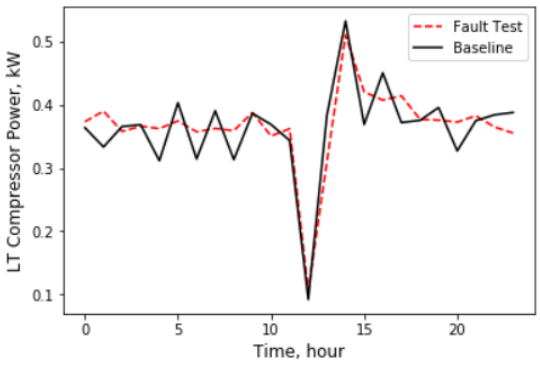

Fig. 4f: LT compressor power consumption

Figure 4. Performance comparison of a baseline test and fault test 2.

2.2.3 Fault Test 3: LT display case expansion valve failure

In this test, the LT display case expansion valve is deliberately forced to close fully or to a nearly closed position during test period. The operational conditions for both the baseline test and the fault test are as follows: -25.6 °F (−32°C) of LT compressor suction refrigerant temperature setpoint, −6°F (−21°C) of LT display case discharge air temperature setpoint, 16 °F (-8.9 °C) of MT compressor suction refrigerant temperature setpoint, 30°F (−1.1°C) of MT display case discharge air temperature setpoint and 72°F (22°C) of Indoor air temperature.

The following changes in the measured variables were observed, as shown in Fig. 5, when LT display case expansion valve fault being throttled.

- LT expansion valve failure interrupts the refrigerant supply to the LT display case, the LT evaporator supply/return air temperature (Fig. 5a and 5b) and the LT compressor suction and superheat temperature (Fig. 5g and Fig. 5h) immediately rise and go out of control. Similarly, the air temperature difference across the LT evaporator drops (Fig. 5c) and the LT evaporator approach temperature (Fig. 5j) increases immediately.

- The immediate impact of the LT expansion valve failure on condenser performance is not obviously due to the relatively small LT cooling load compared to the MT load. Both the air temperature difference the across condenser (Fig. 5d) and the condenser approach temperature (Fig. 5i) are unchanged compared with the baseline case.

- Fig.5e shows that the MT compressor discharge temperature drops while the discharge pressure (Fig.5f) does not change.

- The LT compressor power drops to a minimal level in which the LT compressor works to maintain the suction pressure with no cooling demand. The impact on the MT compressor power is unnoticeable.

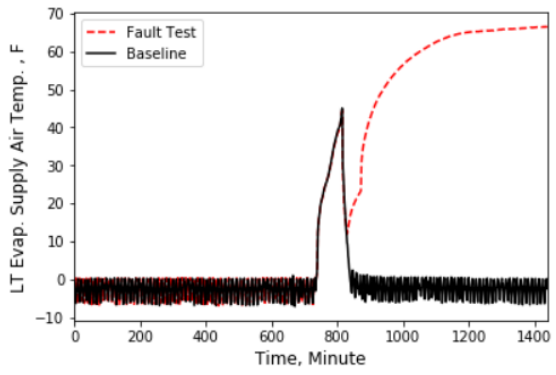

Fig. 5a: LT evaporator supply air temperature

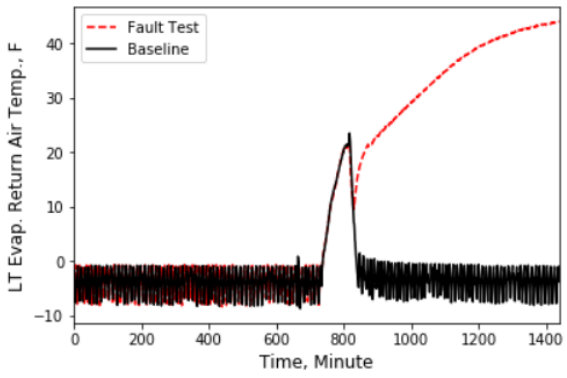

Fig. 5b: LT evaporator supply/return air temperature

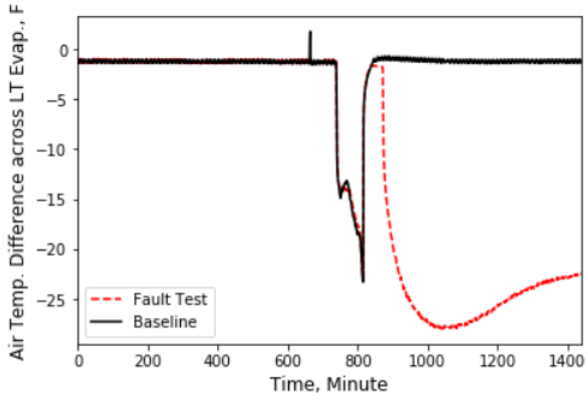

Fig. 5c: Air temperature drop/rise across evaporator

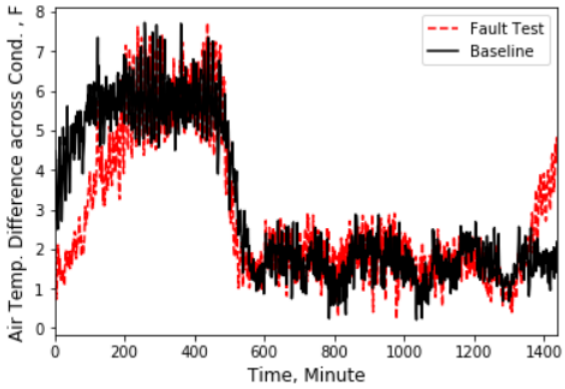

Fig. 5d: Air temperature drop/rise across condenser

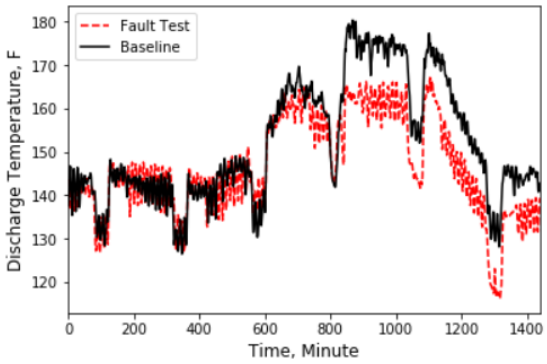

Fig. 5e: MT compressor discharge temperature

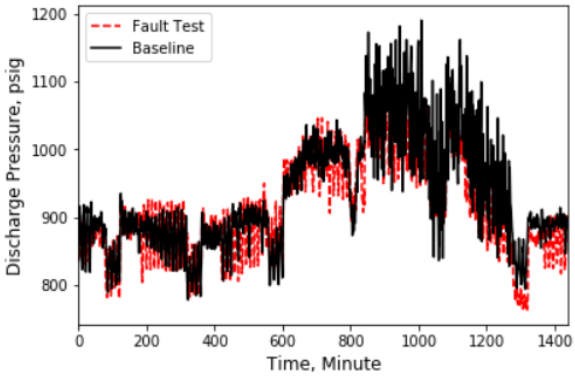

Fig. 5f: MT compressor discharge pressure

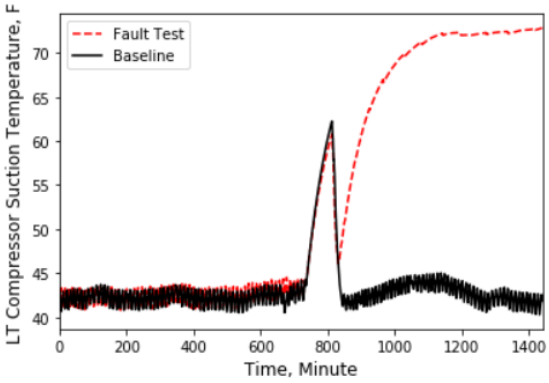

Fig. 5g: LT compressor suction temperature

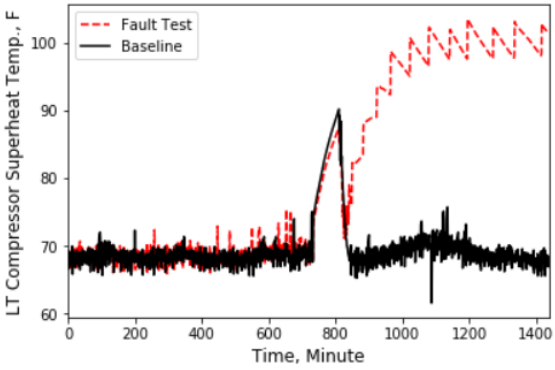

Fig. 5h: LT compressor superheat temperature

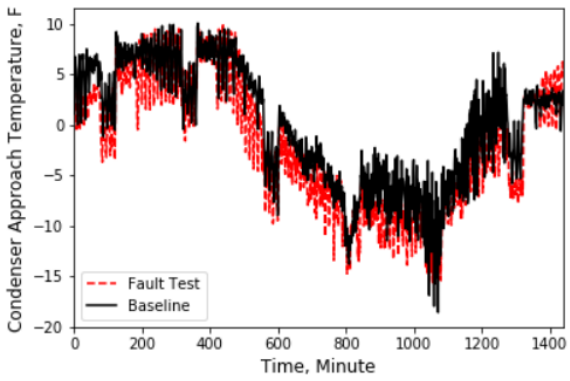

Fig. 5i: Condenser approach temperature

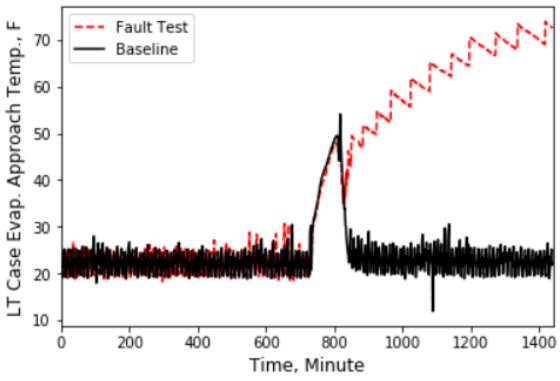

Fig. 5j: LT evaporator approach temperature

Figure 5. Performance comparison of a baseline test and fault test 3.

2.2.4 Fault Test 4: MT display case evaporator fan failure

Fan motor failure is another popular issue for supermarket refrigeration system. To replicate this fan failure, one of the two MT display case evaporator fans is turned off during the test period. The experimental results, as shown in Fig. 6, indicate that the most influenced variables by MT display case evaporator fan failure is the MT evaporator supply air temperature,

- With the failure of one MT evaporator fan, the MT evaporator supply air temperature increases immediately due to the reduction of heat transfer in of the corresponding section of the evaporator coil (Fig. 6a). The supply air sensor is located downstream of and very close to the evaporator coil.

- The MT evaporator return air temperature increases shortly after the evaporator fan failure and then maintains the setpoint again (Fig. 6b). One reason is that the display case cooling load demand is unchanged. In response to the return air rise, the system controls increase the refrigerant mass flow rate to compensate for the cooling lost due to the failure of one of the evaporator fans.

Other performance variables related to the condenser and compressor, such as the air temperature difference across the condenser, the MT compressor suction temperature and superheat temperature, the condenser and the MT evaporator approach temperature, and the LT and MT compressor power consumption are well maintained at the desired values with little deviation from baseline performance.

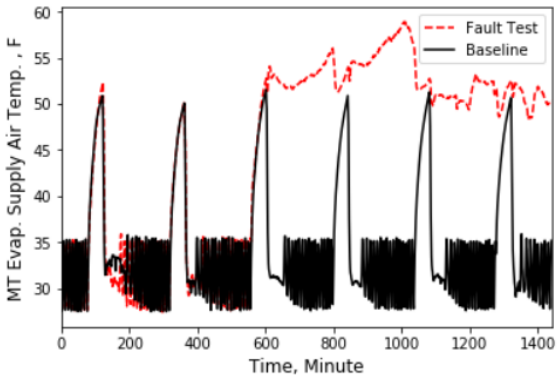

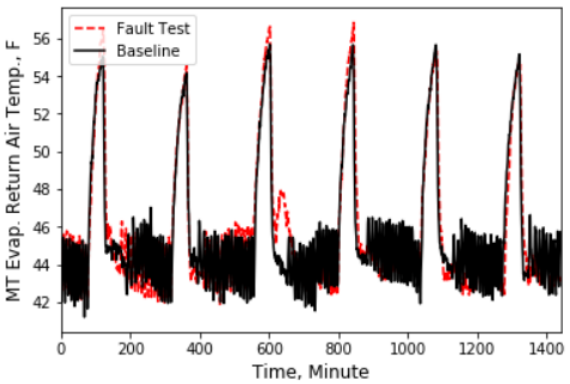

Fig. 6a: MT Evaporator Supply Air Temperature

Fig. 6b: MT Evaporator Return Air Temperature

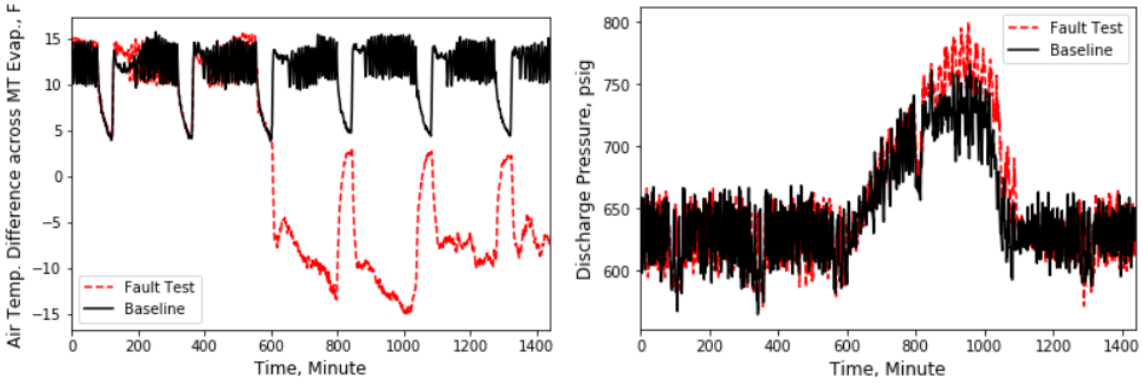

Fig. 6c: Air temperature drop/rise across evaporator

Fig. 6d: MT compressor superheat temperature

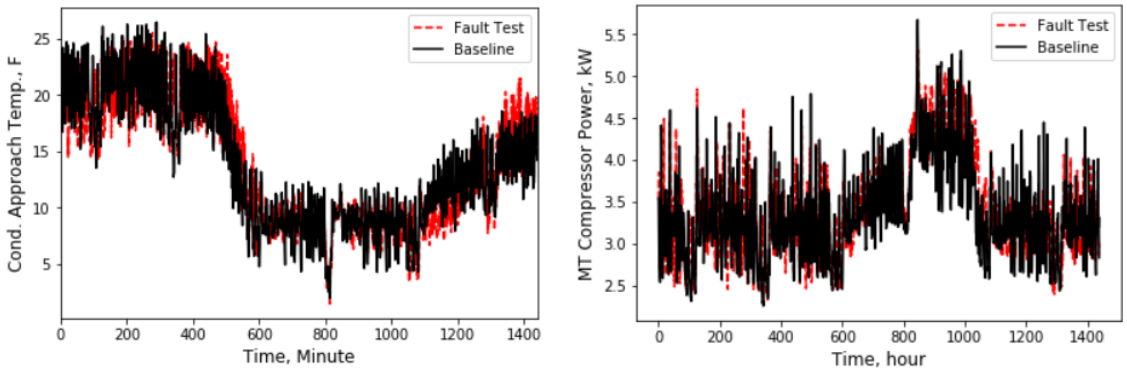

Fig. 6e: Condenser approach temperature

Fig. 6f: MT compressor power consumption

Figure 6. Performance comparison of a baseline test and fault test 4.

2.3 FDD CHARACTERISTICS MATRIX

To summarize the four common faults test results, a FDD characteristics matrix is developed to provides qualitative rules for the detection of tested faults, and can be used to develop practical FDD strategies in future work, such as a decision tree method, to detect and diagnosis faults that occur during the actual operation of supermarket refrigeration systems.

Table 3. FDD Characteristics Matrix

Temperature Control Operation Period	LT display case door open		Ice accumulation in LT evap.	LT expansion valve failure	MT Evap. fan failure
	Normal Operation	Defrost Period			
Compressor					
LT Comp. suction temp.	↓	↓	→	↑↑	→
LT Comp. power	↑	→	→	↓↓	→
MT Comp. discharge temp.	↑	→	→	↓	↑

MT Comp. discharge Pressure	↑	→	→	→	→
MT Comp. power	N/A	N/A	→	→	→
Evaporator					
LT Evap. Supply air temp.	→	↑↑	↑↑	↑↑	N/A
LT Evap. Supply air temp. high limit	N/A	↑↑	N/A	N/A	N/A
LT Evap. Return air temp.	↑	↑	→	↑↑	N/A
LT Evap. Return air temp. high limit	N/A	↑	N/A	N/A	N/A
Air temp. difference across LT evap.	↑	↓↓	↑↑	↓↓	N/A
LT Evap. Approach temp.	↑	↑	→	↑↑	→
LT Evap. Leaving superheat temp.	↓	→	↓		→
MT Evap. Supply air temp.	N/A	N/A	N/A	N/A	↑↑
MT Evap. Return air temp.	N/A	N/A	N/A	N/A	→
Air temp. difference across MT evap.	N/A	N/A	N/A	N/A	↓↓
MT Evap. Approach temp.	N/A	N/A	N/A	N/A	→
MT Evap. Leaving superheat temp.	N/A	N/A	N/A	↑↑	N/A
Condenser					
Air temp. difference across cond.	→	→	→	→	→
Condenser approach temp.	↓	↓	→	→	→

Notes

NA: the variable is not relevant to the fault.

→: the variable is unchanged or has negligible change.

↑ or ↓: the variable has moderate changes: increasing or decreasing

↑↑ or ↓↓: the variable has significant changes: increasing or decreasing

3. MODELING AND SIMUALITON STUDY

In addition to the experimental approach, modeling and simulation, for example computational fluid dynamic (CFD) modeling, has been also used to address the challenges faced by the proposed vaccine distribution solution: refrigeration storage container with vaccine dry-ice package. The modeling and simulation can not only provide a visualization of the temperature distribution in the container, but also offer an optimal distribution of the boxes with an economic cost. The modeling results can provide guidance of experimental setups to save both time and cost.

3.1 MODELING METHODS

The system diagram of the transcritical CO2 refrigeration system is shown in **Error! Reference source not found.**. This is a two-stage system with low- and medium-temperature cooling. The specifications of the components (e.g., compressors, display case, gas cooler condenser) are shown in the previous report [26]. The experiments were conducted within 24 hours. The measurement points are summarized in [26].

For this methodology, the authors first studied the baseline (fault-free) measurement data, from which a baseline model was calibrated. After that, the baseline and fault measurement datasets were investigated, from which the fault models were developed. For the next step, FDD logics (which are used for FDD identifications) were developed. Last, the fault models were deployed into the PythonEMS environment for FDD purposes. **Error! Reference source not found.** shows the overall framework for this study.

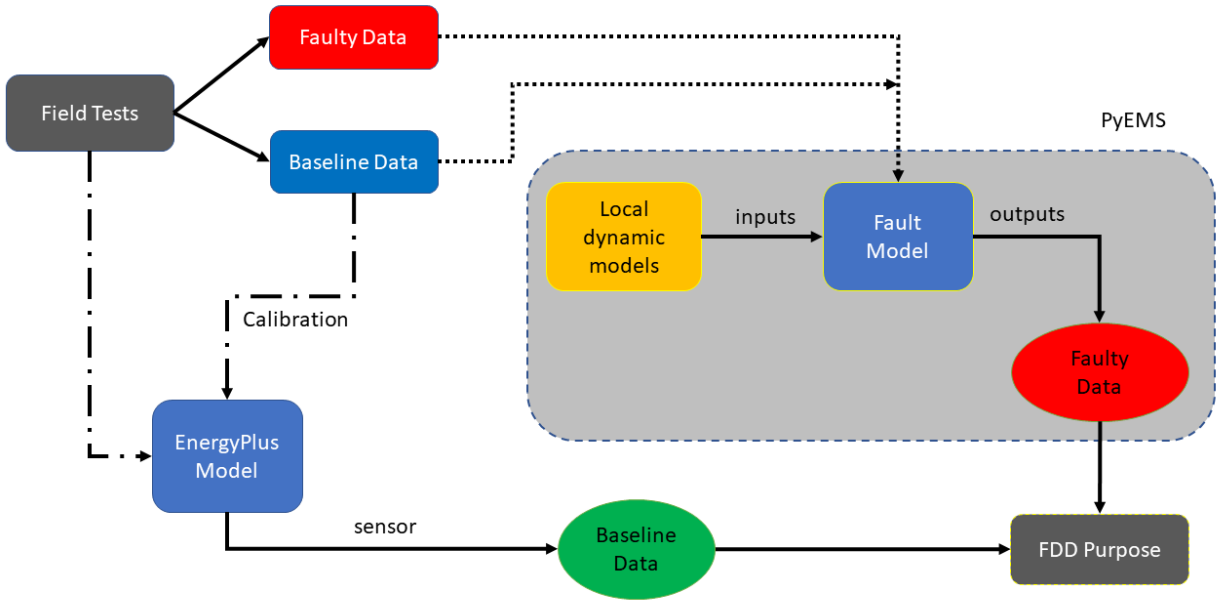

Figure 7. Fault model development framework

3.2 BASELINE MODEL

The baseline model is the model without faults. It is composed of two types of compressors: low-temperature compressors and medium-temperature compressors. The metrics for the compressors are cooling capacity and power consumption.

Low-temperature compressor

The low-temperature compressor always operates at subcritical conditions. The equation is given as.

$$z = a_1 + a_2 T_o + a_3 P_{gc} + a_4 T_o^2 + a_5 T_o P_{gc} + a_6 P_{gc}^2 + a_7 T_o^3 + a_8 P_{gc} T_o^2 + a_9 T_o P_{gc}^2 + a_{10} P_{gc}^3 , \quad (1)$$

Where,
T_o is the *saturated* suction temperature (°C),
T_c is the *saturated* discharge temperature (°C),
z is cooling capacity (W) or power consumption (KW), and
$a_1 \sim a_{10}$ are the coefficients of the performance curve.

Medium-temperature compressor

The medium-temperature compressor operates at both subcritical and supercritical conditions. When the outdoor air temperature is less than 88°F, the compressor will go subcritical, and when the outdoor air temperature higher than or equal to 88°F, it will go supercritical.

The supercritical equation is given as

$$z = a_1 + a_2 T_o + a_3 P_{gc} + a_4 T_o^2 + a_5 T_o P_{gc} + a_6 P_{gc}^2 + a_7 T_o^3 + a_8 P_{gc} T_o^2 + a_9 T_o P_{gc}^2 + a_{10} P_{gc}^3 , \quad (2)$$

Where

T_o is the *saturated* suction temperature (°C),
T_c is the *saturated* discharge temperature (°C),
Z is cooling (W) or power consumption (KW),
P_{gc} is the gas cooler pressure (bar), and
$a_1 \sim a_{10}$ are the coefficients of the performance curve.

The baseline models provide crucial insights for the dominant parameters determining cooling capacity and power consumption for CO2 refrigeration systems. The fault models were developed by mimicking the idea of baseline models.

$$z = a_1 + a_2 T_o + a_3 T_c + a_4 T_o^2 + a_5 T_o T_c + a_6 T_c^2 + a_7 T_o^3 + a_8 T_c T_o^2 + a_9 T_o T_c^2 + a_{10} T_c^3 . \quad (3)$$

3.3 FAULT MODELS

Five faults were selected for modeling because they are among the most common faults for supermarket refrigeration cases: (1) ice accumulation in the evaporator coil, (2) evaporator fan partial failure, (3) expansion valve failure, (4) display door open, and (5) condenser blockage.

3.3.1 Fault symptoms

The following paragraphs discuss the effects of the different fault symptoms: ice accumulation on evaporator coil, evaporator fan partial failure, expansion valve failure, ice accumulation on evaporator coil, display door open, condenser blockage. They will degrade the performance of refrigeration systems from both air side and refrigerant side.

Ice accumulation on evaporator coil

On the air side, the ice will reduce the heat transfer effect of coil and thus the overall heat transfer coefficient will decrease. This fault will drive the compressor to run faster to maintain the desired set points of supply air temperature (SAT) or the set points of food temperature. This type of situation will lead to more power demands for compressors.
On the refrigerant side, the refrigerant temperature right after the evaporator coil may be lower than under normal conditions due to less heat gains from the air side. Thus, the refrigerant might not fully evaporated or saturated with a gaseous state. Under severe fault conditions, the mixture of liquid and gases might enter the compressor and cause damage.

Evaporator fan partial failure
On the air side, the supply air flow rate will decrease; therefore, the heat transfer quantity will be decreased. On the refrigerant side, the same issue will occur with the ice accumulation on evaporator coil model. Similarly, with the ice accumulation on evaporator coil model, this fault might drive the compressor to run faster to maintain the desired set points. This fault can be detected easily with an airflow sensor.

Expansion valve failure
This fault will directly affect the refrigerant side. Normally, the purpose of the expansion valve is to reduce the pressure and temperature of the refrigerant after the condenser. Once the system is running under fault condition, the refrigerant will carry higher than normal pressure and temperature. When the refrigerant goes through the evaporator coil, the heat transfer effect will be reduced. Thus, the SAT will be higher than normal.

Display door open
This fault is mainly imposed through the air side. When the display door is open, the indoor air (with a higher temperature) around the display case will enter through the evaporator coil. If the cooling coil capacity is not high enough, the SAT will rise, even if the compressor is running at full speed. If the cooling coil capacity is high enough, the compressor speed will go higher to maintain the food temperature.

Condenser blockage
This fault acts on the system on the air side. The purpose of the condenser is to cool down the refrigerant coming from the compressor upstream. It transfers the heating energy from the evaporator coil to the outdoor environment. Once the system is running under faults, the refrigerant temperature will be higher than normal. Then the refrigerant will go through the expansion valve with a higher temperature and, subsequently, the evaporator coil. Because of the higher temperature of the refrigerant, the heat transfer amount carried over is reduced. Therefore, the SAT and food temperature will be compromised.

3.3.2 Fault model equation

The following assumptions were made for the fault models:
(1) The faulty condition cooling capacity is smaller than or equal to the baseline (fault-free) condition.
(2) The faulty condition power consumption is higher than or equal to the baseline (fault free) condition.

(3) The SAT of display case is higher than or equal to the baseline (fault free) condition.
(4) The fault intensity is the intensity (or severity) of fault introduced by humans (e.g., a customer forgets to close the door of the display case) or occurred naturally due to degradation (e.g., refrigerant leaks because the pipe eroded). This measurement indicates the severity (or fault magnitude) of the fault, and the input perturb parameter is introduced as the cause of the fault. A system may have more than one fault.
(5) The cooling impact ratio is the ratio between faulty cooling capacity and baseline cooling capacity. This ratio could be an empirical value, a measurement from a historical operation.
(6) The rated parameters are the ideal variables under nominal or normal conditions without faults, such as cooling capacity, SAT, and power.

For supermarket refrigeration systems, power consumption and the SAT are the most important parameters because power consumption is directly related to operation costs and the SAT is directly related to food quality and revenue. Thus, the fault models focus on two outputs—power consumption and the SAT. The fault models for both are based on inputs: fault intensity, cooling impact ratio, faulty saturated suction temperature, faulty saturated condensing temperature, rated power consumption, and the set of coefficients. For faulty saturated suction temperature and faulty condensing temperature, a few extra measurements are required to construct the local dynamic models. The development of local dynamic models is shown in equations (4) through (11). **Error! Reference source not found.** demonstrates the components of the proposed fault models.

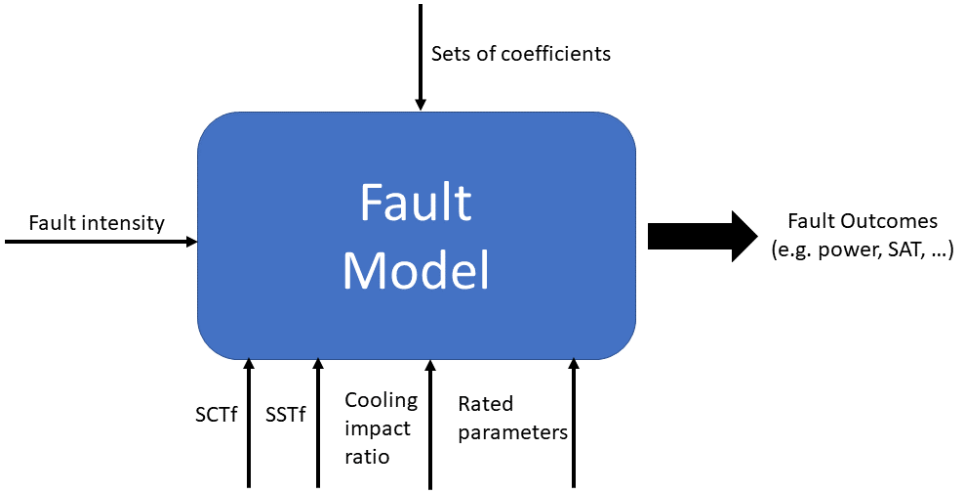

Figure 8. Fault model components.

For the cooling capacity of the display case, the lumped parameter model is shown for the baseline in

$$\dot{Q}_o = (UA)_o \times (T_{SS} - T_{ra})_o \,. \tag{4}$$

Similarly, the faulty condition cooling capacity is:

$$\dot{Q}_f = (UA)_f \times (T_{SS} - T_{ra})_f \,. \tag{5}$$

The ratio of the above two cooling capacity terms is expressed as

$$\frac{\dot{Q}_f}{\dot{Q}_o} = \frac{(UA)_f \times (T_{SS} - T_{ra})_f}{(UA)_o \times (T_{SS} - T_{ra})_o} . \quad (6)$$

A cooling impact ratio for the cooling capacity is defined as

$$\varepsilon = \frac{\dot{Q}_f}{\dot{Q}_o} \leq 1 \quad . \quad (7)$$

Another dimensionless number is the fault intensity

$$f_i = \frac{(UA)_f}{(UA)_o} \leq 1 . \quad (8)$$

The formula is given as

$$\frac{\varepsilon}{f_i} = \frac{(T_{SS} - T_{ra})_f}{(T_{SS} - T_{ra})_o} \quad . \quad (9)$$

When fault occurs at the evaporator side for the two faults chosen, the saturated suction temperature tends to increase compared with nominal conditions. Similarly, the return air temperature (RAT) tends to increase when compared with nominal conditions.

Thus, the faulty saturated suction temperature is given as

$$T_{SS_f} = \frac{\varepsilon}{f_i}(T_{SS} - T_{ra})_o \; + \; T_{ra_f} . \quad (10)$$

Following a similar approach, equations for the faulty saturated condensing temperature can be derived as,

$$T_{SS_f} = \frac{\varepsilon}{f_i}(T_{SC} - T_{oa})_o \; + \; T_{oa_f} . \quad (11)$$

The fault modes are given as follows:

Low-temperature compressor power fault model:

$$\frac{W_f}{W_n} = 1 + f_i \times \left\{ c_0 \operatorname{atan}\left(\frac{T_{ss}}{273.15} + 1\right) + c_1\left(\operatorname{atan}\left(\frac{T_{ss}}{273.15} + 1\right)\right)^2 + c_2\left(\operatorname{atan}\left(\frac{T_{sc}}{273.15} + 1\right)\right) + c_3\left(\operatorname{atan}\left(\frac{T_{sc}}{273.15} + 1\right)\right)^2 + c_4(f \right.$$
. (12)

Medium-temperature compressor power fault model:

$$\frac{W_f}{W_n} = 1 + f_i \times \left\{ c_0 \operatorname{atan}\left(\frac{T_{ss}}{273.15} + 1\right) + c_1\left(\operatorname{atan}\left(\frac{T_{ss}}{273.15} + 1\right)\right)^2 + c_2\left(\operatorname{atan}\left(\frac{T_{sc}}{273.15} + 1\right)\right) + c_3\left(\operatorname{atan}\left(\frac{T_{sc}}{273.15} + 1\right)\right)^2 + c_4(f \right.$$
(13)

Low-temperature compressor SAT Fault Model:

$$\frac{SAT_f}{SAT_n} = 1 + f_i \times \left\{ c_0 \operatorname{atan}\left(\frac{T_{ss}}{273.15} + 1\right) + c_1\left(\operatorname{atan}\left(\frac{T_{ss}}{273.15} + 1\right)\right)^2 + c_2\left(\operatorname{atan}\left(\frac{T_{sc}}{273.15} + 1\right)\right) + c_3\left(\operatorname{atan}\left(\frac{T_{sc}}{273.15} + 1\right)\right)^2 + c_4(f \right.$$
. (14)

Medium temperature compressor SAT fault model:

$$\frac{SAT_f}{SAT_n} = 1 + f_i \times \left\{c_0 \operatorname{atan}\left(\frac{T_{ss}}{273.15} + 1\right) + c_1\left(\operatorname{atan}\left(\frac{T_{ss}}{273.15} + 1\right)\right)^2 + c_2\left(\operatorname{atan}\left(\frac{T_{ss}}{273.15} + 1\right)\right)^3 + c_3\left(\operatorname{atan}\left(\frac{T_{sc}}{273.15} + 1\right)\right) + c_4\left(a\right.\right. \quad (15)$$

3.4 MODEL CALIBRATION AND VALIDATION

This section presents the results for this fault study, including the baseline field test dataset, fault measurement dataset, and fault model calibrations, fault model implementations in simulation environment, and FDD investigation with fault models. The baseline is the scenario without faults. For the fault dataset, there are five faults are investigated: (1) ice accumulation on evaporator coil, (2) evaporator fan partial failure, (3) expansion valve failure, (4) display door open, and (5) condenser blockage.

3.4.1 Validation of baseline models and measurement data

Error! Reference source not found. demonstrates the measurement dataset and modeling results for the baseline model. The red lines denote the measurement dataset. The blue lines represent the modeling results. The top plot shows that the power consumption of the low-temperature compressor is close to the modeling results. In practical field tests, the CO2 refrigeration systems are not operated in 100% efficiency, thus leading to small biases between the measurement dataset and modeling results. The bottom plot is for the medium-temperature compressor. Discrepancies also exist between the field test datasets and modeling due to the nonoptimal running conditions (e.g., outdoor air temperature). However, the overall trends are synced well between the measurement and modeling results for the medium-temperature compressor.

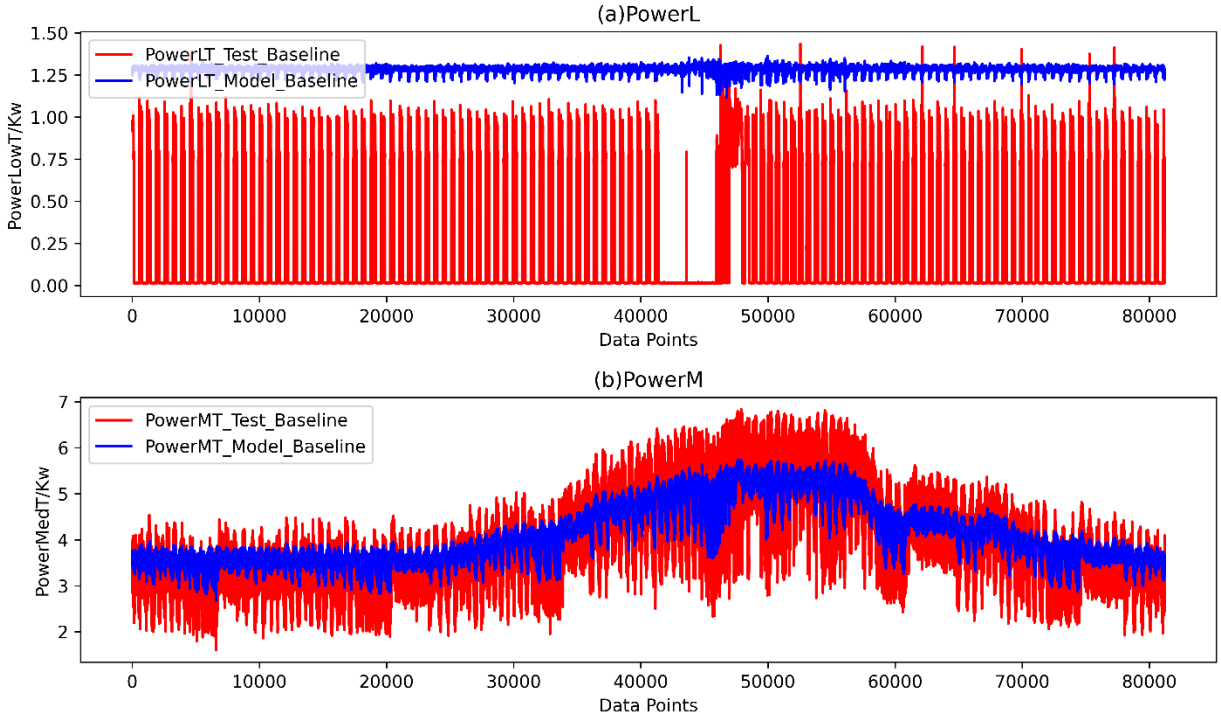

Figure 9. Comparison of the baseline measurement and model.

3.4.2 Faults' measurement data study

For the fault measurement dataset, there are five faults are investigated: (1) ice accumulation on evaporator coil, (2) evaporator fan partial failure, (3) expansion valve failure, (4) display door open, and (5) condenser blockage. This section demonstrated the analysis for the fault measurement data. The red lines represent the normal case, and the blue lines denote the faulty case. For each row, the left subplot is for the low-temperature compressor, and the right subplot is for the medium-temperature compressor.

3.4.3 Calibration of faults models using measurement data

This subsection demonstrates the calibrations of fault models based on measurement datasets. There are five faults are investigated: (1) ice accumulation on evaporator coil, (2) evaporator fan partial failure, (3) expansion valve failure, (4) display door open, and (5) condenser blockage. The red lines denote the fault measurement dataset, and the blue lines represent the fault modeling dataset. The upper row subplots show the power consumption for low- and medium-temperature cases, respectively. The bottom row subplots show the SAT for low- and medium-temperature cases, respectively. The RMSE is used to quantify the discrepancies between measurement and modeling results.

3.4.3.1 Ice accumulation on evaporator coil

Error! Reference source not found.1 demonstrates the comparison of fault model results and fault measurement datasets for the ice accumulation on evaporator fault. The root-mean-squared-error (RMSE) is used to check the modeling agreement with measurement dataset. Both of the low-temperature and medium-temperature cases power consumption are in good agreement. For the SAT, the fault model also closely follows the patterns captured from measurement dataset.

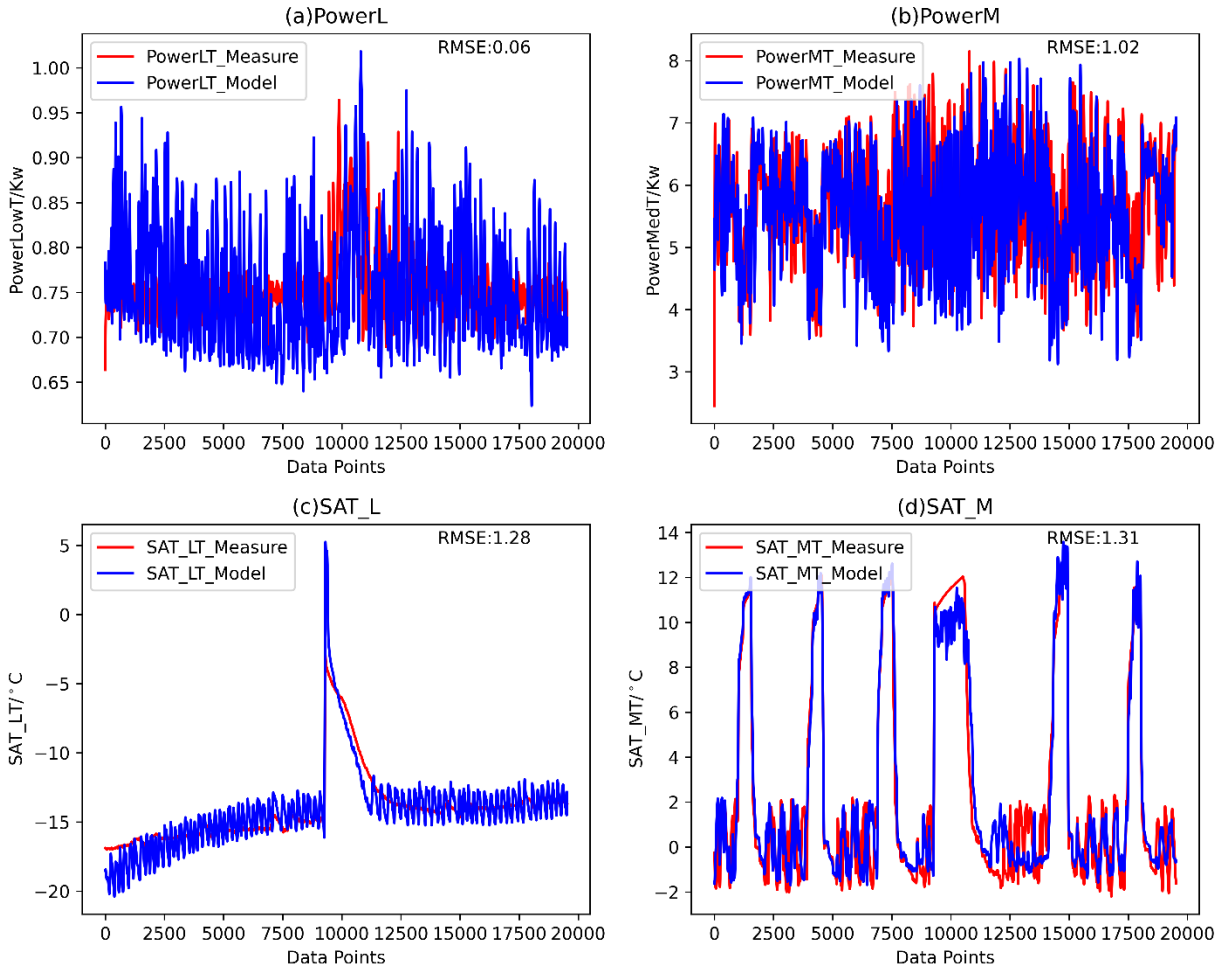

Figure 10. Calibration of ice accumulation for the evaporator fault

3.4.3.2 Evaporator fan partial failure

Error! Reference source not found.Error! Reference source not found. demonstrates the comparison of fault model results and fault measurement datasets for the evaporator fan partial failure fault. As shown in the plots, the RMSEs are both acceptable. Both of power consumption and supply-air-temperature are in good agreement between fault models and measurement dataset.

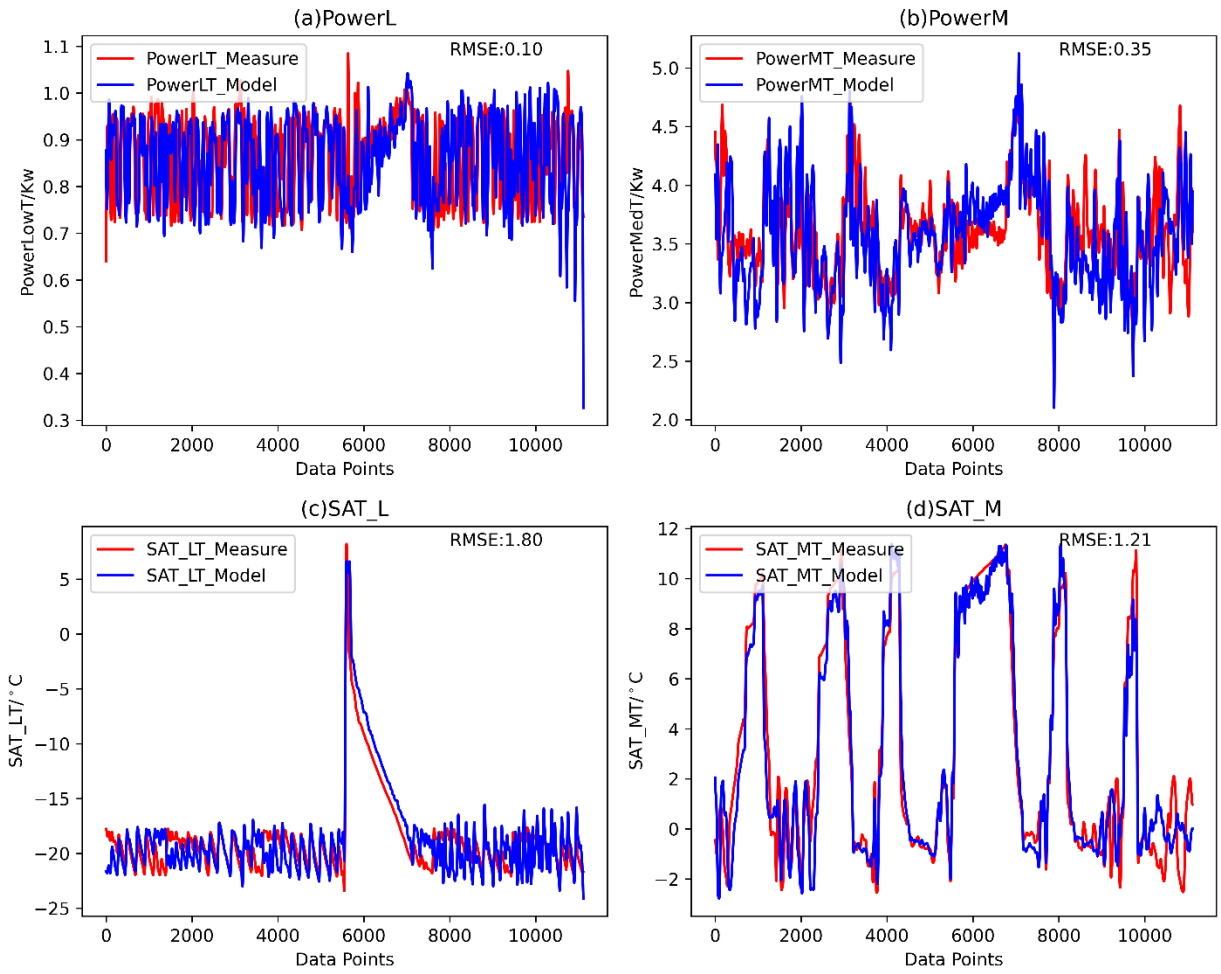

Figure 11. Calibration for the evaporator fan partial failure fault.

3.4.3.3 Expansion valve failure

Error! Reference source not found.3 **Error! Reference source not found.**demonstrates the comparison of fault model results and fault measurement datasets for the expansion valve failure fault. As shown in the plots, the RMSEs are both acceptable. For power consumption, the fault modeling results are close to measurement dataset. For supply air temperature prediction of medium temperature display case, the fault model lacks dynamics compared with the measurement data. However, the RMSE indicates it is acceptable for the SAT.

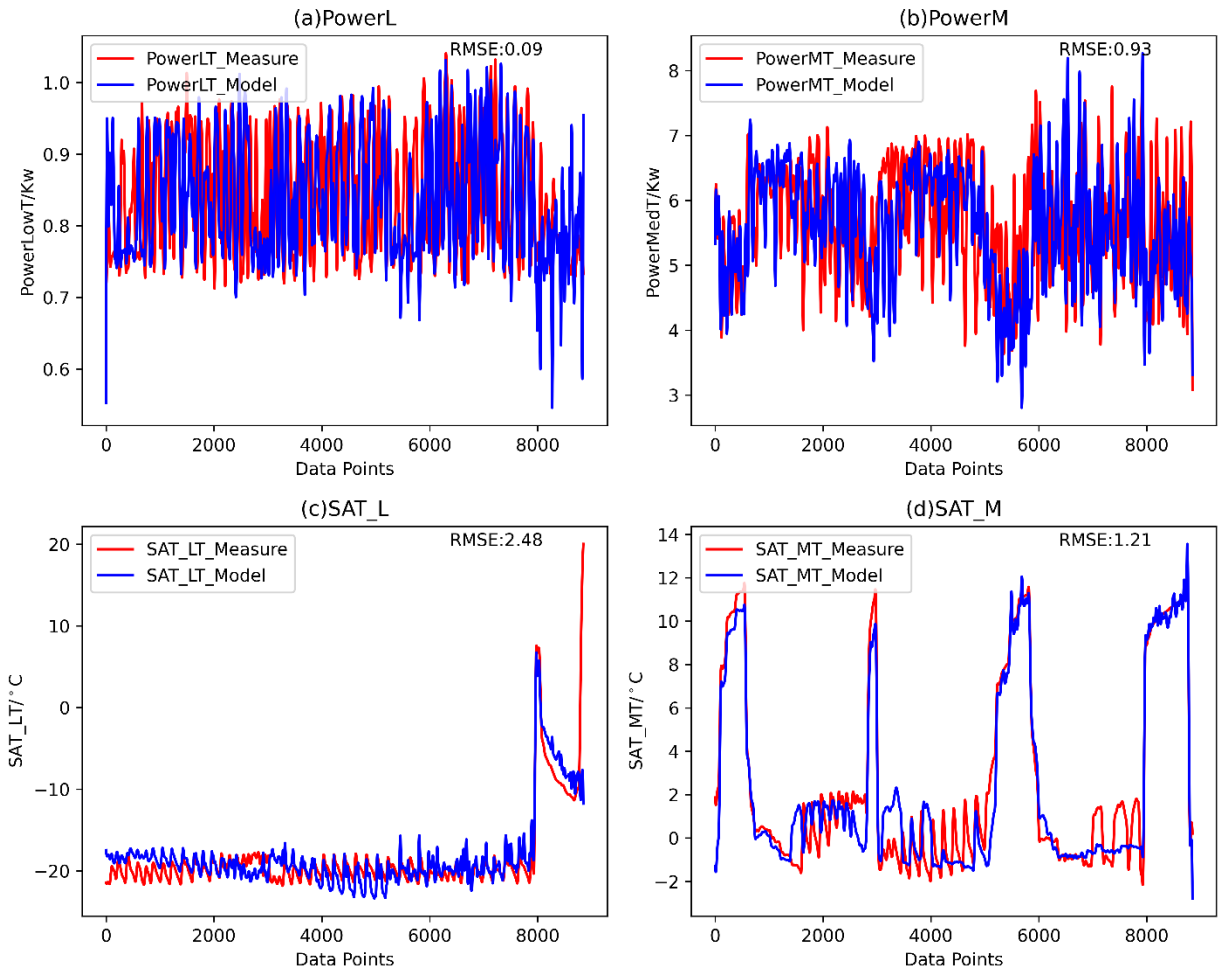

Figure 12. Calibration for the expansion valve failure fault

3.4.3.4 Display door open

Error! Reference source not found.4 **Error! Reference source not found.**demonstrates the comparison of fault model results and fault measurement datasets for the display door open fault. As shown in the plots, the RMSEs are both acceptable. Overall, the fault model results are close to measurement dataset. There are small portions of dataset, where the dynamics are not captured well. This cloud be from the measurement noise, or system dynamics.

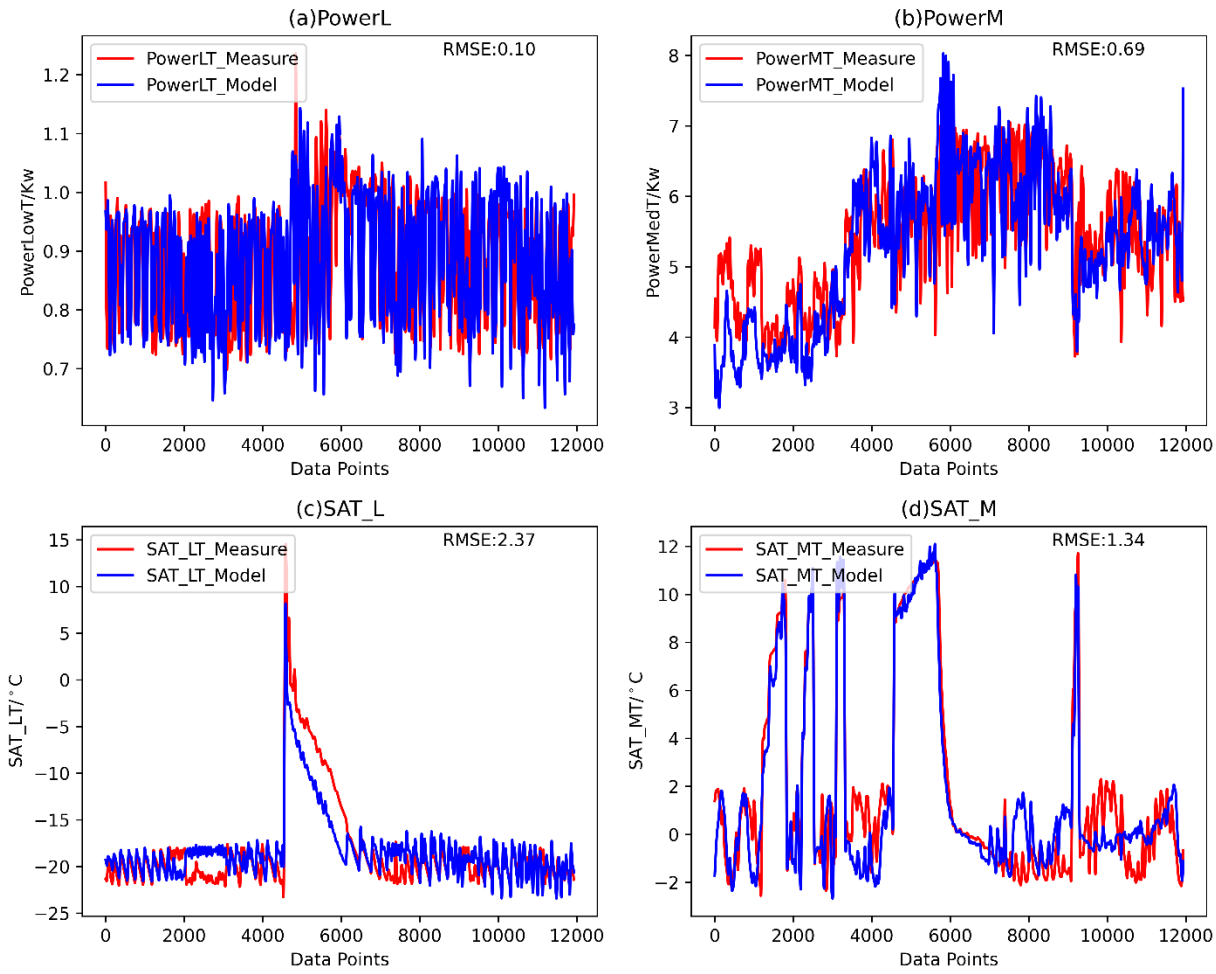

Figure 13. Package with dry ice in test 1.

3.4.3.5 Condenser blockage

Error! Reference source not found.5 **Error! Reference source not found.**demonstrates the comparison of fault model results and fault measurement datasets for the condenser block fault. As shown in the plots, the RMSEs are both acceptable. The power consumption and supply air temperature results agree well between fault model and measurement.

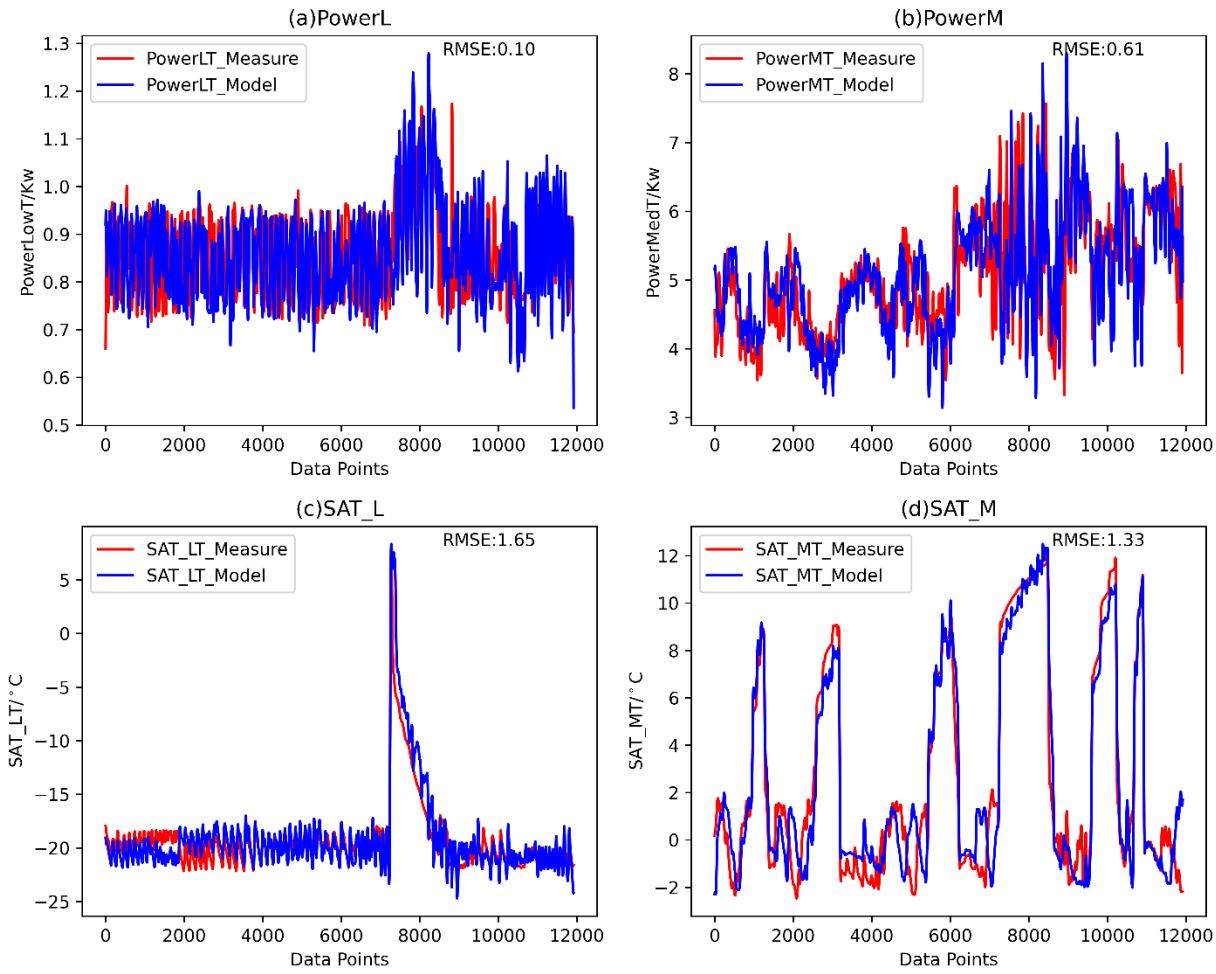

Figure 14. Location of thermocouple in the container of test 2.

3.5 IMPLEMENTATION IN PYTHONEMS

This subsection is demonstrating the fault modeling implementation through PythonEMS. There are five faults are investigated: (1) ice accumulation on evaporator coil, (2) evaporator fan partial failure, (3) expansion valve failure, (4) display door open, and (5) condenser blockage. The red lines are the baseline results, and the blue lines are the fault results. Three days of simulation results were retrieved. The top two plots are for the power consumption of low- and medium-temperature cases, respectively. The bottom plots are for the SAT of low- and medium-temperature cases, respectively. Three days of simulations are implemented.

3.5.1 Ice accumulation on evaporator coil

Error! Reference source not found.6 demonstrates the fault modeling results in the EnergyPlus environment for the ice accumulation on evaporator coil fault. As shown in the plots, a larger difference exists between baseline and faulty cases. The fault results show higher power consumption compared

with baseline. It is similar for supply air temperature. Furthermore, with SAT decreasing, the power consumption increases. This indicates the refrigeration is working harder to achieve the setpoints, from modeling perspective.

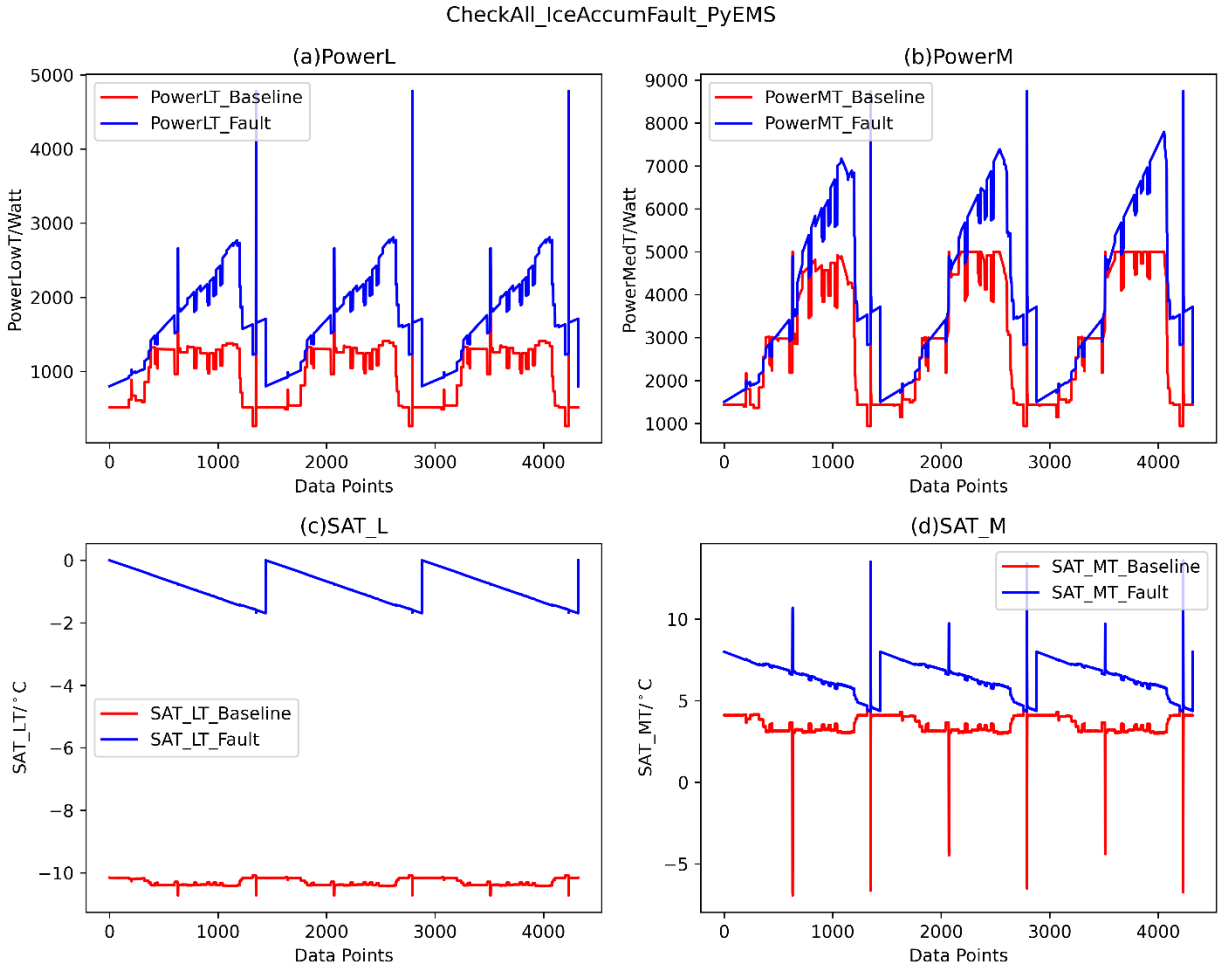

Figure 15. EnergyPlus implementation for the ice accumulation on evaporator fault

3.5.2 Evaporator fan partial failure

Error! Reference source not found.7Error! Reference source not found. demonstrates the fault modeling results in the EnergyPlus environment for the evaporator fan partial failure fault. The red lines are the baseline results, and the blue lines are the fault results. Three days of simulation results were retrieved. The top two plots are for the power consumption of low- and medium-temperature cases, respectively. The bottom plots are for the SAT of low- and medium-temperature cases, respectively. As shown in the plots, a larger difference exists between baseline and faulty cases. The fault case shows higher values for power consumption and supply air temperature, compared with baseline.

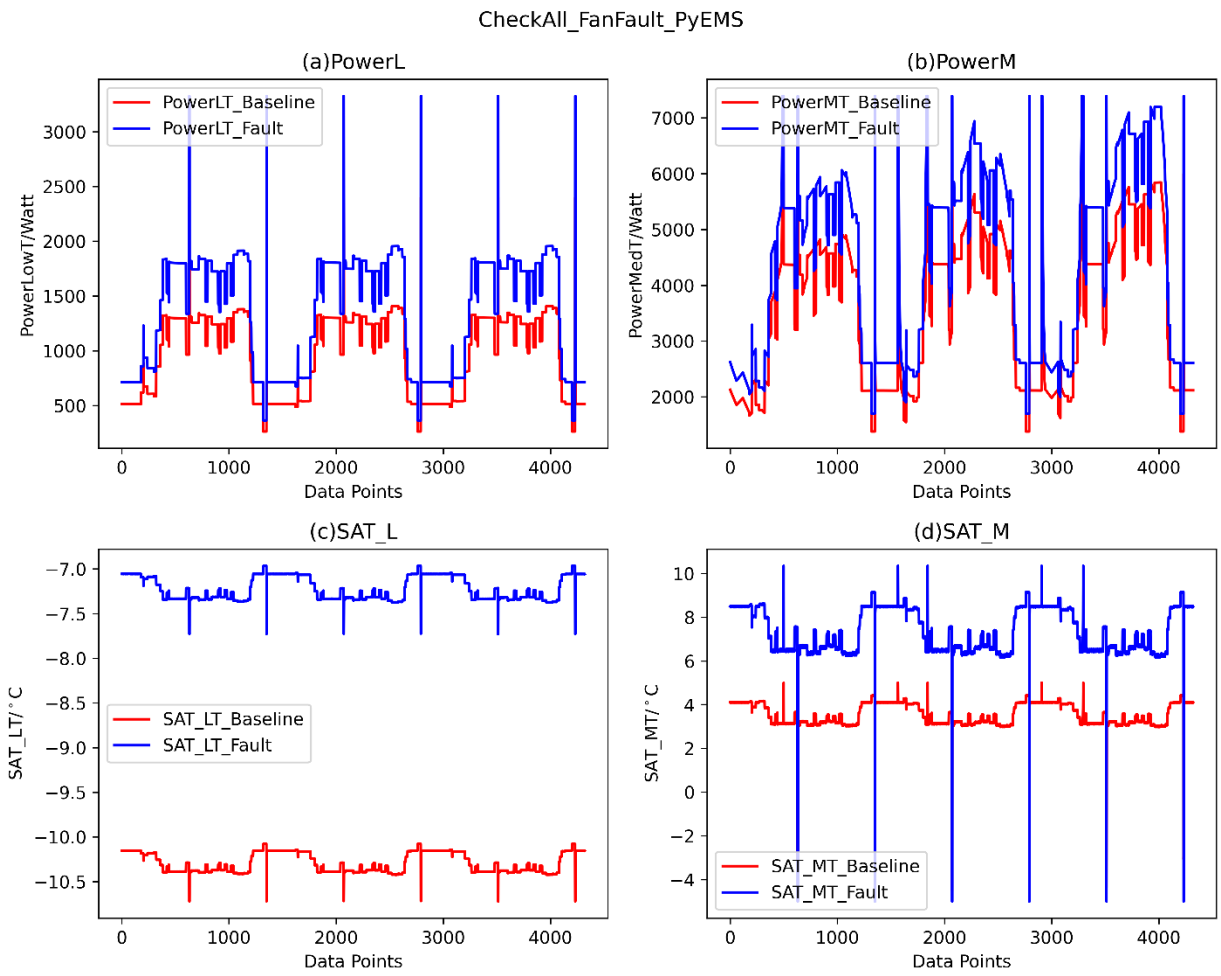

Figure 16. EnergyPlus implementation for the evaporator fan partial failure fault.

3.5.3 Expansion valve failure

Error! Reference source not found.8 demonstrates the fault modeling results in the EnergyPlus environment for the expansion valve failure fault. The red lines are the baseline results, and the blue lines are the fault results. Three days of simulation results were retrieved. The top two plots are for the power consumption of low- and medium-temperature cases, respectively. The bottom plots are for the SAT of low- and medium-temperature cases, respectively. As shown in the plots, a larger difference exists between the baseline and faulty cases. This fault behaviors are similar with ice accumulation on evaporator coil. With supply air temperature decreasing, the power consumption increases. The faulty SAT never achieves the baseline SAT.

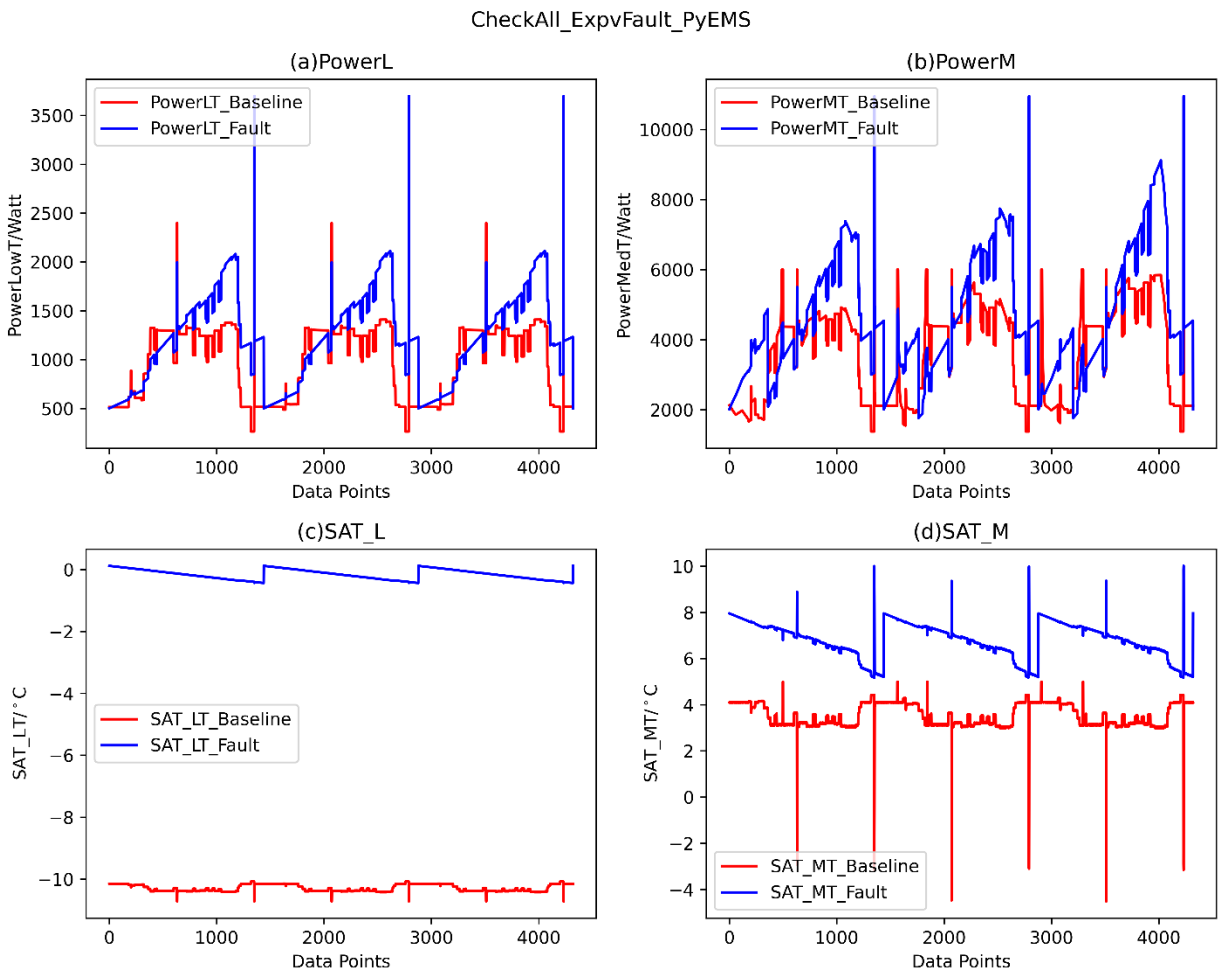

Figure 17. EnergyPlus implementation for the expansion valve failure fault

3.5.4 Display door open

Error! Reference source not found.9 demonstrates the fault modeling results in the EnergyPlus environment for the display door open fault. The red lines are the baseline results, and the blue lines are the fault results. Three days of simulation results were retrieved. The top two plots are for the power consumption of low- and medium-temperature cases, respectively. The bottom plots are for the SAT of low- and medium-temperature cases, respectively. As shown in the plots, a larger difference exists between baseline and faulty cases. Similarly with expansion valve failure, the power consumption and SAT of fault models are higher than baseline.

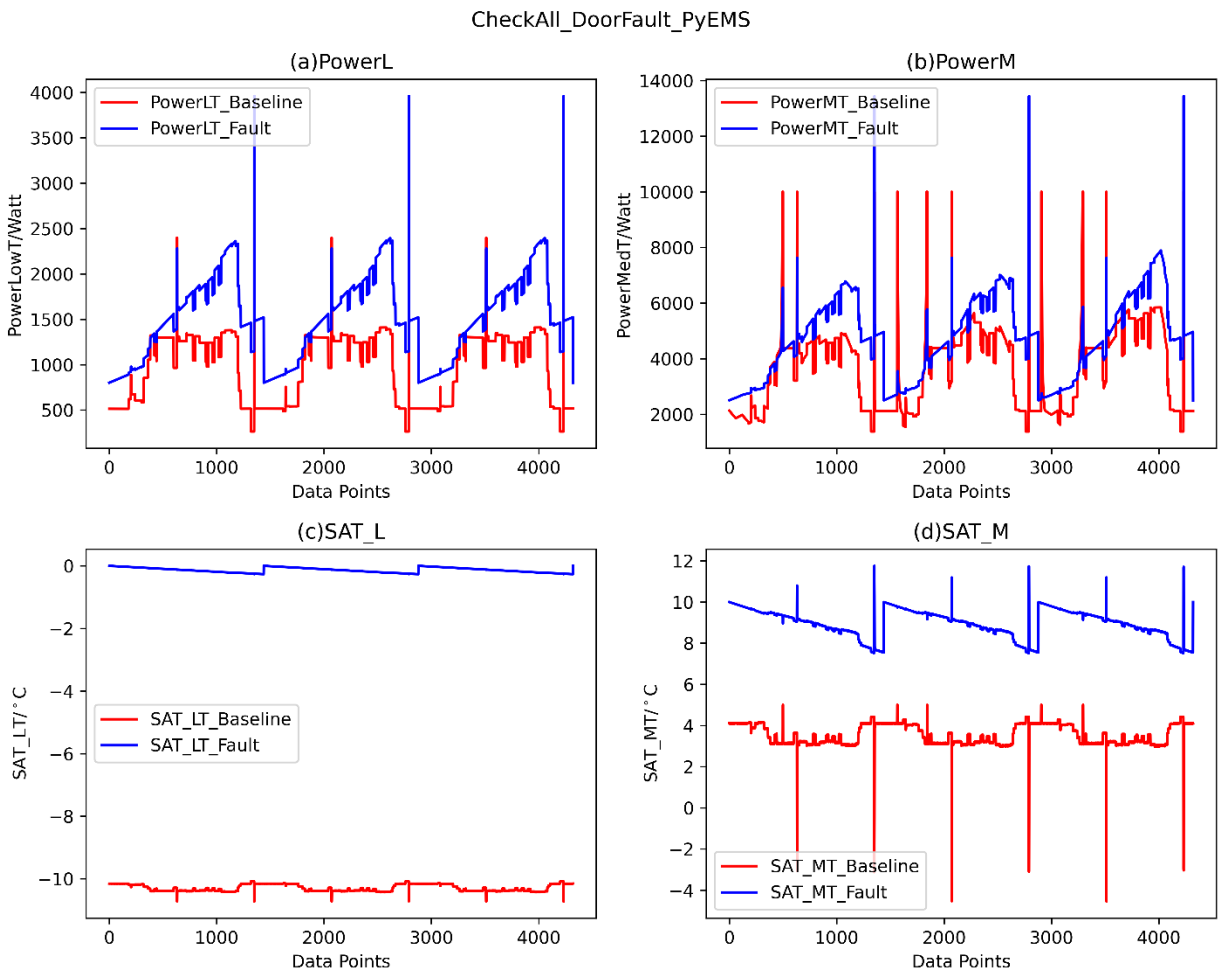

Figure 18. EnergyPlus implementation for the display door open fault.

3.5.5 Condenser blockage

Error! Reference source not found.20 demonstrates the fault modeling results in the EnergyPlus environment for the condenser blockage fault. The red lines are the baseline results, and the blue lines are the fault results. Three days of simulation results were retrieved. The top two plots are for the power consumption of low- and medium-temperature cases, respectively. The bottom plots are for the SAT of low- and medium-temperature cases, respectively. As shown in the plots, a larger difference exists between baseline and faulty cases.

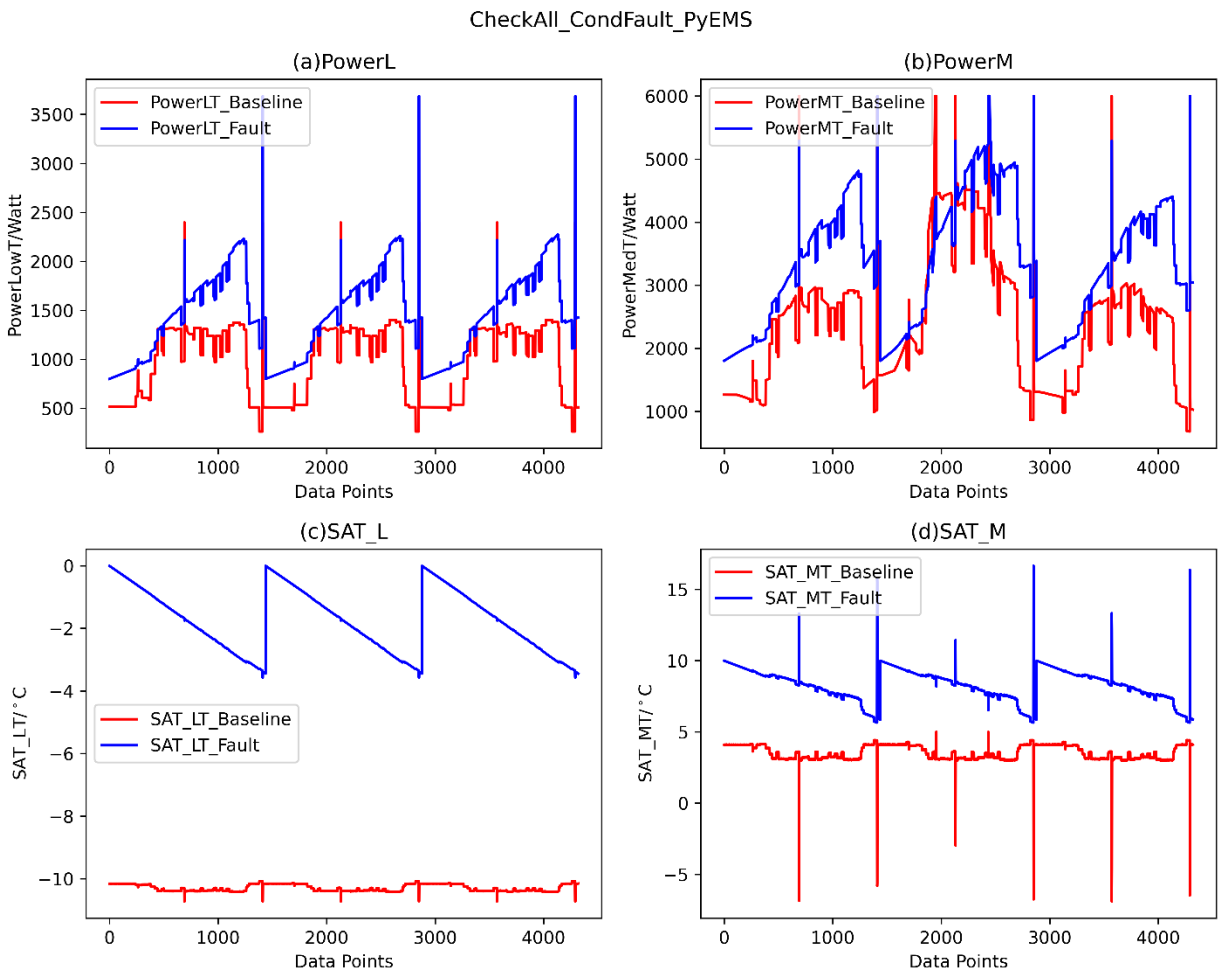

Figure 19. EnergyPlus implementation for the condenser blockage fault.

4. FAULT DETECTION AND DIAGNOSTICS

The purpose of fault model development is to do fault detection and diagnostics (FDD) in the systems. FDD algorithm is developed based on measurement data. FDD implementation for both measurement and simulation data is performed.

4.1 FDD ALGORITHM

Detecting faults for CO2 refrigeration systems is complicated. Thus, the authors developed an FDD flow chart based the field tests (**Error! Reference source not found.**1). The principle of FDD is shown in **Error! Reference source not found.**2. The FDD is obtained based on measurement data from both the air and refrigerant sides. Compressor faults are not included in this study. Based on the FDD flow chart, seven different indicators exist:

- 0: No fault
- 1: Evaporator fan fault
- 2: Display case door fault
- 3: Expansion valve fault
- 4: Condenser fault or compressor fault
- 5: Condenser fan fault
- 6: Evaporator fault

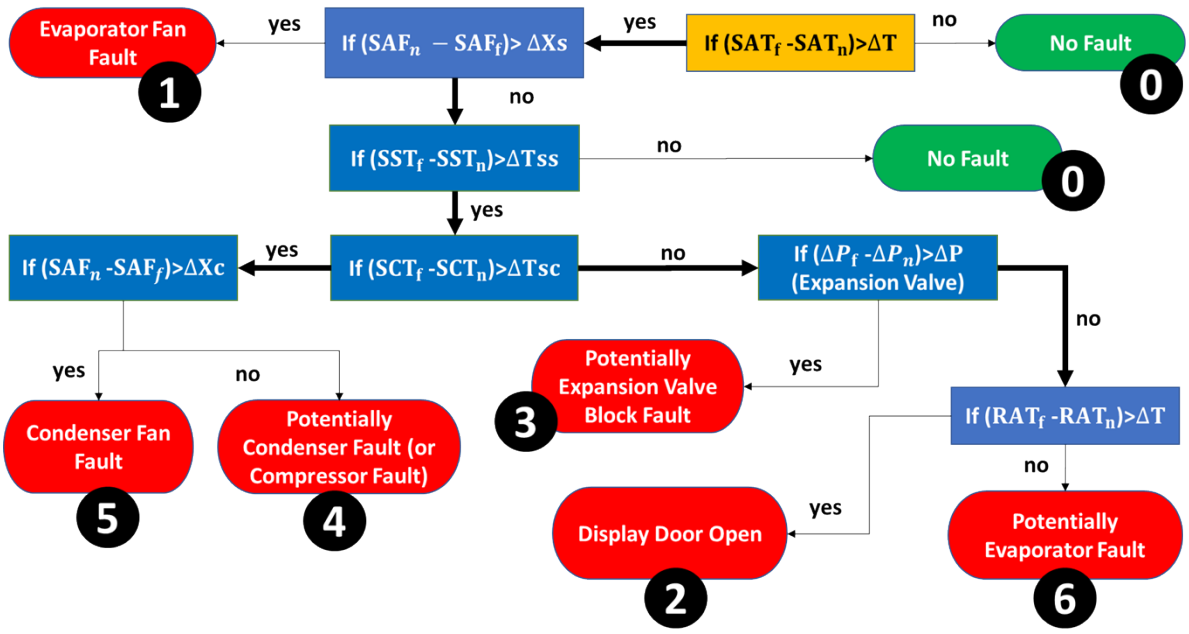

Figure 20. FDD flow chart

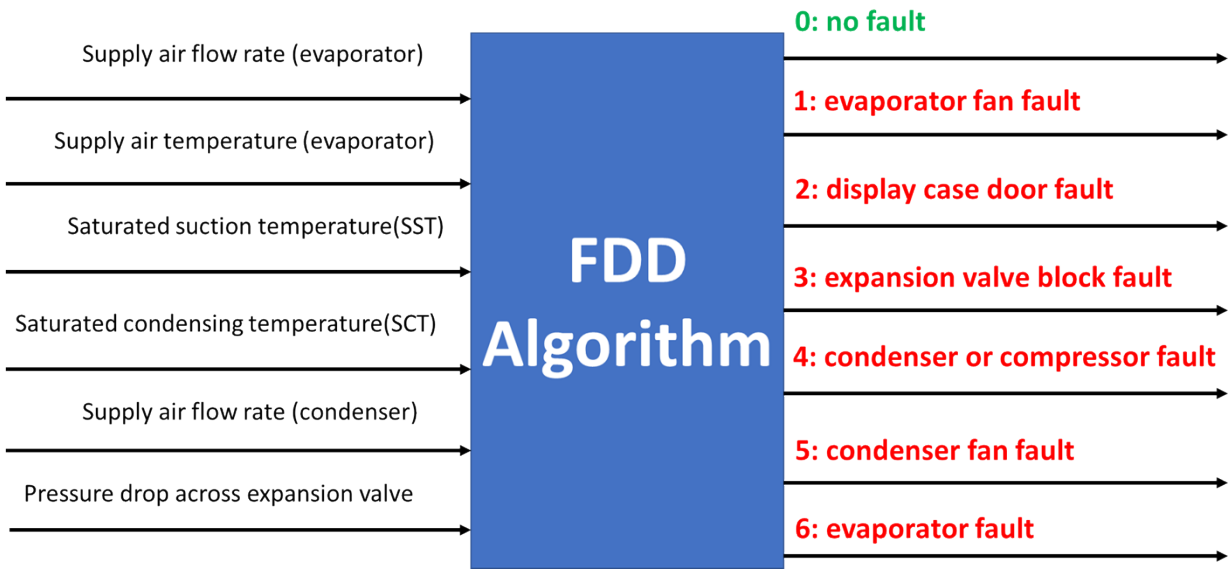

Figure 21. FDD principle

4.2 FDD FOR MEASUREMENT DATASET

Error! Reference source not found.3 demonstrates the FDD results for the measurement data for the five faults investigated. The FDD value of "0" denotes the fault-free condition. The FDD value of greater than 0 indicates the fault types as proposed from the FDD algorithm.

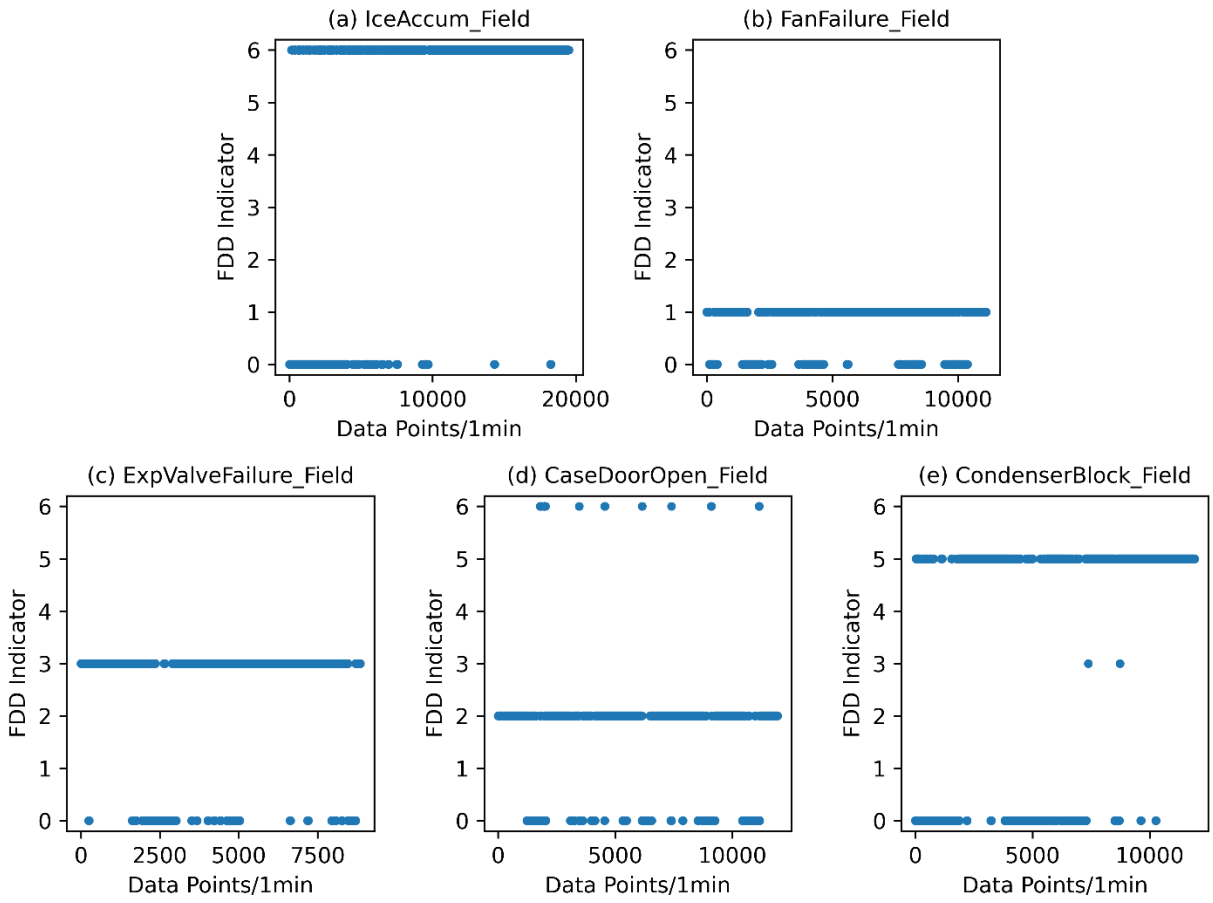

Figure 22. FDD for the fault measurement data

Error! Reference source not found.3 shows that higher than 90% of data points are detected successfully for the measurement faults. This indicates the robustness of the proposal FDD algorithms. On the other hand, there is noisy in measurement data, which leads to less than 100% detection of faults. It is expected to have better FDD detection accuracy with more measurement data for other types of variables.

4.3 FDD IN SIMULATION ENVIRONMENT

Error! Reference source not found.4 demonstrates the FDD results for the simulated data for the five faults investigated. The FDD value of "0" denotes the fault-free condition. The FDD value of greater than 0 indicates the fault types as proposed from the FDD algorithm. Based on simulation data, the FDD shows 100% detection of faults.

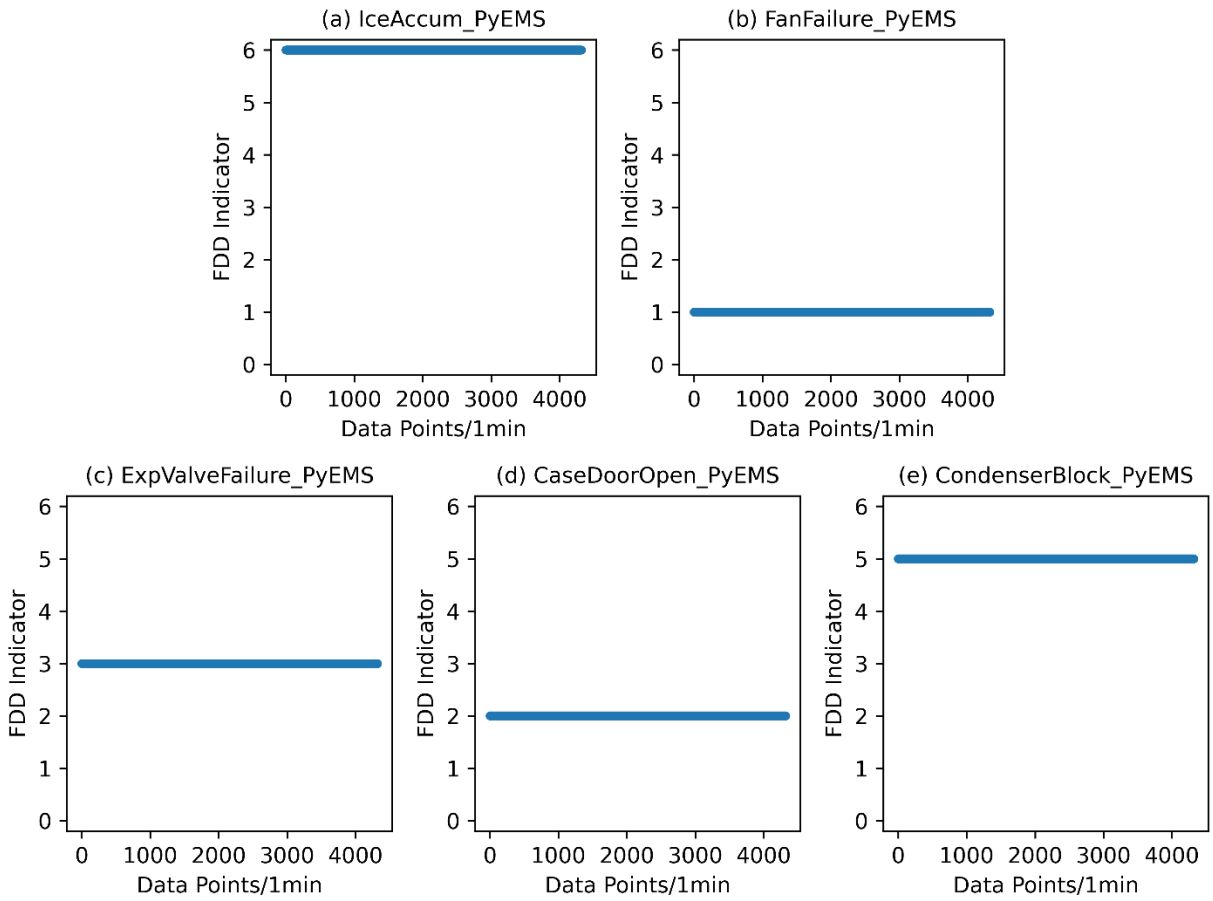

Figure 23. FDD for the fault modeling results

5. CONCLUSIONS AND RECOMMENDATIONS

In this paper, we purposely created different operational faults in a laboratory-scale commercial refrigeration system and investigated the impact of these faults on the operation and performance of the refrigeration system. To summarize the impact of these four faults on refrigeration system performance, an FDD characteristics matrix is given in Table 4. The experimental results revealed the following key indicators for each of the faults.

- LT display case door open: The LT evaporator return air temperature, the air temperature difference across the LT evaporator and the LT evaporator approach temperature immediately rises. The LT compressor suction temperature and superheat temperature decrease. During the defrost cycle, both the supply and return air temperatures rise and reach higher temperature limits than the baseline case. The air temperature difference across the LT evaporator under defrost conditions increases.

- LT display case evaporator ice accumulation: The LT evaporator supply air temperature and the air temperature difference across the LT evaporator increase. The LT evaporator approach temperature and condenser approach temperature slightly decrease.

- LT display case expansion valve failure: The LT evaporator supply/return air temperature, the LT compressor suction and superheat temperature, and the LT evaporator approach temperature immediately rise. The air temperature difference across the LT evaporator and the MT compressor discharge temperature decrease.

- MT display case evaporator fan failure: The MT evaporator supply air temperature increases immediately due to the loss of heat transfer in the corresponding section of the evaporator coil. The MT evaporator return air temperature increases for a short period of time after the evaporator fan failure and then maintains the setpoint again.

This study also demonstrates results from the fault models developed and calibrated for supermarket transcritical CO2 refrigeration systems. The study involved four steps. five fault models regarding the power consumption and SAT were proposed for low- and high-temperature cases, respectively. Next, the fault models were calibrated with field tests, and the modeling accuracies were in good agreement with the measurement dataset based on the RMSE. The fault models were then implemented in PythonEMS of the EnergyPlus platform as the model-based study. Last, the FDD was executed based on the developed fault models, which had good agreement with the measurement data. Overall, the fault models work as expected.

In addition, several topics listed as below can be future work：

- Further development of more accurate fault models, such as adding component-based fault models
- Developing high-fidelity dynamic refrigeration models is highly desirable
- Deploying the proposed fault models in the actual CO2 refrigeration equipment for field study.

6. ACKNOWLEDGMENTS

Funding for this research was provided by the US Department of Energy, Office of Energy Efficiency and Renewable Energy. The authors would like to thank Erika Gupta, Samuel Petty and Ed Vineyard, Program Managers of Building Technologies Office, Antonio Bouza, Program Managers of Advanced Manufacturing Office , for their support of this work.

7. REFERENCES

1. US EPA 2008, Energy Star Building Upgrade Manual. Chapter 11: Facility Type: Supermarkets and Grocery Stores. US EPA Office of Air and Radiation. http://www.energystar.gov/sites/default/files/buildings/tools/EPA_BUM_CH11_Supermarkets.pdf
2. Navigant Consulting 2009, Energy Savings Potential and R&D Opportunities for Commercial Refrigeration. Final Report submitted to US Department of Energy, Energy Efficiency and Renewable Energy, Building Technologies Program. September 23, 2009
3. Booten, C., Sparn,B., Maguire, J., Balamurugan, S.P., Duoba, M., Canosa,A.F., Munk, J., Kuruganti, T., Sun, J., Cui, B., Dong, J., Development and Evaluation of Distributed Energy Resource Device Models: Electric Vehicles, Electric Water Heaters, and Commercial Refrigeration Systems, United States: N. p., 2020. Web. doi:10.2172/1660063.
4. Kim M-H, Pettersen J, Bullard CW. Fundamental process and system design issues in CO2 vapor compression systems. Progress in Energy and Combustion Science 2004;30:119–74.
5. Ge YT, Tassou SA. Thermodynamic analysis of transcritical CO2 booster refrigeration systems in supermarket. Energy Conversion and Management 2011;52:1868–75.
6. Hafner A, Försterling S, Banasiak K. Multi-ejector concept for R-744 supermarket refrigeration. International Journal of Refrigeration 2014;43:1–13.
7. da Silva A, Bandarra Filho EP, Antunes AHP. Comparison of a R744 cascade refrigeration system with R404A and R22 conventional systems for supermarkets. Applied Thermal Engineering 2012;41:30–5.
8. BehFar, A., Yuill, D., & Yu, Y., Automated fault detection and diagnosis methods for supermarket equipment (RP-1615). Science and Technology for the Built Environment 23, 1253–1266 (2017).
9. BehFar, A., Yuill, D., & Yu, Y., Automated fault detection and diagnosis methods for supermarkets – method selection, replication, and applicability, Energy & Buildings, 198 (2019) 520—527.
10. Yang, Z., Rasmussen, K.B., Kieu, A.T., Izadi-Zamanabadi, R., Fault Detection and Isolation for a Supermarket Refrigeration System – Part One: Kalman-Filter-Based Methods, IFAC Proceedings Volumes, Volume 44, Issue 1, 2011; Pages 13233 – 13238.
11. Yang, Z., Rasmussen K.B., Kieu, A.T., Izadi-Zamanabadi, R., Fault Detection and Isolation for a Supermarket Refrigeration System – Part Two: Unknown-Input-Observer Method and Its Extension, IFAC Proceedings Volumes, Volume 44, Issue 1, 2011, Pages 4238-4243.
12. Kim, M., Kim, M.S., 2005, Performance investigation of a variable speed vapor compression system for fault detection and diagnosis, International Journal of Refrigeration 28, 481–488.
13. Tassou, S.A., Grace, I.N., 2005, Fault diagnosis and refrigerant leak detection in vapour compression refrigeration system, International Journal of Refrigeration 28, 680–688.
14. Zhao, X., Yang, M., Li, H., 2014, Field implementation and evaluation of a decoupling-based fault detection and diagnostic method for chillers, Energy and Buildings 72, 419–430.
15. Kocyigit, N., Bulgurca, H., Lin, C.X., 2014, Fault diagnosis of a vapor compression refrigeration system with hermetic reciprocating compressor based on p-h diagram, International Journal of Refrigeration 45, 44–54.
16. BehFar, A., Yuill, D., Yu, Y., 2018, Supermarket system characteristics and operating faults (RP-1615), Science and Technology for the Built Environment 24, 1104–1113.

17. Yu, Y., Woradechjumroen, D., Yu, D., 2014, A review of fault detection and diagnosis methodologies on air-handling units, Energy and Buildings, V82:p550-562
18. Katipamula, S., & Brambley, M.R., 2005, Methods for fault detection, diagnostics, and Prognostics for building systems—A Review, Part I, HVAC&R Research, 11:1, 3-25
19. Katipamula, S., Brambley, M.R., 2005. Methods for fault detection, diagnostics, and prognostics for building systems—a review, part II. HVAC&R Research 11(2):169-87
20. Kim, W., & Katipamula, S., 2018 A review of fault detection and diagnostics methods for building systems, Science and Technology for the Built Environment, 24:1, 3-21
21. Li Y, O'Neill Z. A critical review of fault modeling of HVAC systems in buildings. Building Simulation, vol. 11, Springer; 2018, p. 953–75.
22. Zhang L, Wen J, Li Y, Chen J, Ye Y, Fu Y, et al. A review of machine learning in building load prediction. Applied Energy 2021;285:116452.
23. Li P, Qiao H, Li Y, Seem JE, Winkler J, Li X. Recent advances in dynamic modeling of HVAC equipment. Part 1: Equipment modeling. HVAC&R Research 2014;20:136–49.
24. Li P, Li Y, Seem JE, Qiao H, Li X, Winkler J. Recent advances in dynamic modeling of HVAC equipment. Part 2: Modelica-based modeling. HVAC&R Research 2014;20:150–61.
25. Li Y, O'Neill Z, Zhang L, Chen J, Im P, DeGraw J. Grey-box modeling and application for building energy simulations-A critical review. Renewable and Sustainable Energy Reviews 2021;146:111174.
26. Fricke, B., and Sharma, V., 2016, High efficiency, low emission refrigeration system, ORNL report, ORNL/TM-2016/363, CRADA/NFE-11-03296, Oak Ridge National Laboratory (ORNL); 2016